

# Amber force field implementation, molecular modelling study, synthesis and MMP-1/MMP-2 inhibition profile of (*R*)- and (*S*)-*N*-hydroxy-2-(*N*-isopropoxybiphenyl-4-ylsulfonamido)-3-methylbutanamides<sup>☆</sup>

Tiziano Tuccinardi,<sup>a</sup> Adriano Martinelli,<sup>a,\*</sup> Elisa Nuti,<sup>a</sup> Paolo Carelli,<sup>a</sup> Federica Balzano,<sup>b</sup> Gloria Uccello-Barretta,<sup>b</sup> Gillian Murphy<sup>c</sup> and Armando Rossello<sup>a,\*</sup>

<sup>a</sup>Dipartimento di Scienze Farmaceutiche, Università di Pisa, via Bonanno 6, 56126 Pisa, Italy

<sup>b</sup>Dipartimento di Chimica e Chimica Industriale, Università degli Studi di Pisa, via Risorgimento, 35, 56126 Pisa, Italy

<sup>c</sup>Department of Oncology, University of Cambridge, Hills Road, Cambridge CB2 2XY, UK

Received 28 November 2005; accepted 24 January 2006

Available online 17 February 2006

**Abstract**—Ab initio calculations (B3LYP/Lan12DZ level of theory) were performed in this study to determine all the structural and catalytic zinc parameters required in order to study MMPs and their complexes with hydroxamate inhibitors by means of the AMBER force field. The parameters thus obtained were used in order to study the docking of some known MMPi (Batimastat, CGS 27023A and Prinomastat) and our previously described inhibitor **a** which had shown an inhibitory activity for MMP-1, and -2, with the aim of explaining the different selectivity. On this basis the two enantiomers (*R*)-**b** and (*S*)-**b** were designed and synthesized, as more potent MMP-2 inhibitors than our previously described inhibitor **a**. Between these two enantiomers the eutomer (*R*)-**b** proved to be 24.7 times and 15.3 times more potent than CGS 27023A and the parent compound **a** on MMP-2, maintaining a higher index of MMP-2/MMP-1 selectivity compared with CGS 27023A and the more potent inhibitor Prinomastat. The hydroxamate (*R*)-**b** can be considered as a progenitor of a new class of biphenylsulfonamido-based inhibitors that differ from compound **a** in the presence of an alkyl side chain on the C alpha atom, and show different potency and selectivity profiles on the two MMPs considered.

© 2006 Elsevier Ltd. All rights reserved.

## 1. Introduction

Metalloproteinases are one of the five catalytic classes of proteinases found in human. All metalloproteinases use a Zn<sup>2+</sup> ion, linked stably to their catalytic site, to effect amide bond hydrolysis on their natural peptide substrates.<sup>2</sup> Several types of zinc enzymes are known and are presently the object of intensive studies, for example, carboxypeptidase A (CPA), histone deacetylases (HDACs), tumour necrosis factor  $\alpha$ -convertase (TACE) and matrix metalloproteinases (MMPs).<sup>3</sup> The human MMP family is known to include at least 23 enzymes,

divided into four sub-groups on the basis of their substrate specificity: collagenases (MMP-1, -8, and -13), gelatinases (MMP-2 and -9), stromelysins (MMP-3, -10, and -11) and membrane-type MMPs (MT-MMPs).<sup>4</sup> MMP activity is highly regulated at many levels and, under normal conditions it is controlled by endogenous inhibitors known as tissue inhibitors of MMPs (TIMPs).<sup>5</sup> Uncontrolled over-expression of MMPs can promote a variety of diseases including arthritis, tumour metastasis, multiple sclerosis and periodontal degradation. On this basis a large number of MMP inhibitors (MMPi) have been developed as potential therapeutic agents.<sup>3–12</sup> Many of the known MMPi contain a zinc-binding group (ZBG) linked to different scaffolds to ensure strong interactions within the co-factor-binding regions of these enzymes; among them the more developed and potent class of MMPi utilizes a hydroxamate as the ZBG.<sup>13–21</sup> Among the MMPs, the two gelatinases (MMP-2 and MMP-9), matrilysin (MMP-7) and MT1-MMP (MMP-14) play a

**Keywords:** Docking; Force field parameters; MMP inhibitors.

<sup>☆</sup> See Ref. 1.

\* Corresponding authors. Tel.: +39 050 2219556; fax: +39 050 2219605 (A.M.); tel.: +39 050 2219562; fax: +39 050 2219605 (A.R.); e-mail addresses: [marti@farm.unipi.it](mailto:marti@farm.unipi.it); [aros@farm.unipi.it](mailto:aros@farm.unipi.it)

significant role in certain key functions of tumour cells, facilitating metastatic tumour dispersion and angiogenesis, resistance to apoptosis and activation of EGF receptors.<sup>22–28</sup> In the past, some potent ‘broad spectrum’ MMPi have been proposed and tested against tumours, but at present none of them are on the market.<sup>10,29</sup> In fact, many of these new molecules have determined a severe musculoskeletal syndrome, with fibroproliferative effects in the joint capsule of the knee.<sup>30–32</sup> These effects are thought to be linked to an impairment of normal tissue remodelling governed by MMP-1 and/or by sheddases such as TNF- $\alpha$ -convertase.<sup>33</sup> For these reasons, a lack of activity with respect to MMP-1 is considered to be an important factor in reducing some of the side effects found for ‘non-selective’ MMPi.<sup>34</sup> The recent development of synthetic MMPi possessing a good potency and selectivity towards the two gelatinases, together with the discovery that some of these molecules active on MMP-2 show important pro-apoptotic effects on tumour cell cultures, confirms the validity of their use as potential anti-tumour agents.<sup>3,7–9,13–21,35–37</sup> Nowadays new compounds possessing a selective inhibitory activity on MMPs that are over-expressed in tumours are in great demand, with particular reference to viability control and invasiveness of the cancer cell, and many groups and pharmaceutical companies all over the world are involved in improved studies on these new synthetic MMPi, not only to develop new drugs but also to discover new agents to be used as diagnostics in cancer.<sup>38,39</sup> As reported above, it has been demonstrated that the catalytic zinc ion in the active pocket of MMPs is directly involved in the degradation of extracellular matrix components. In the latent form of gelatinases, the active site presents the zinc bound to three histidine residues and blocked by the sulfhydryl group of a cysteine. During activation, the detachment of the propeptide also involves the dissociation of this residue, and the active site becomes accessible for the substrate.<sup>40</sup> A mechanism has been proposed for the catalytic activity, on the basis of structural information. In the first step, the zinc ion is tetrahedrally coordinated to three histidines and a water molecule; during proteolysis, the water donates a proton to Glu219 (1HFC<sup>41</sup> sequence number), which transfers it to the nitrogen of the scissile amide bond that is stabilized by Ala182; this is followed by the generation of a salt bridge between Glu219 and the free amine of the cleaved substrate.<sup>42</sup> As the zinc ion plays an important role in the substrate degradation, one of the possible strategies to develop new MMPi is based on the search for the best ZBG able to compete with the substrate in zinc coordination. Common ZBGs of MMPi include hydroxamates, carboxylates, thiolates and phosphonates.<sup>8,43,44</sup> Among these the hydroxamate group has proved to be the most potent (100–2000 times compared with their carboxylate analogue).<sup>43</sup> It is known from crystallographic data that two zinc atoms are present in MMPs: a structural tetra-coordinated atom, which is linked with three histidines and an aspartate with a tetrahedral structure, and a catalytic atom, which, in the presence of hydroxamate inhibitors, is linked to three histidines and the ligand with a penta-coordination in a bipyramidal trigonal geometry, considering that the hydroxamate group behaves like a bidentate ligand.<sup>45–47</sup> Some new *N*-arylsulfonyl-substituted alkoxyaminoaceto-

hydroxamic acid derivatives have recently been synthesized and tested, and proved to possess a good selectivity for MMP-2 over MMP-1;<sup>48</sup> these may be considered as promising leads for the development of new selective inhibitors of metalloproteinases. A rational planning of these inhibitors requires the availability of adequate molecular models, to make possible to study the mechanism of the enzyme–ligand interaction. Resolution of the crystal structure of MMP-2 gave researchers the opportunity to develop new compounds by means of a structure-based approach; so far, however, no X-ray structures of the MMP-2-inhibitor complexes have been reported, and there is a real need for theoretical studies on the binding mode of MMP-2 with its inhibitors, since they can provide insight into the interaction occurring in the active site. In order to perform the docking of ligands with metalloproteinases, the use of computational methods has proved to be problematic, because of the restrictions imposed by the presence of the zinc ion. These applications are developed on the basis of an empirical force field, which cannot be used directly in the design of ZBGs of MMPs<sup>49</sup> and other metalloproteinases, given the lack of parameters relating to the metallic ions. The use of generalized parameters in the case of these ions is highly unadvisable, considering that the coordination bonds formed by these ions largely depend on the nature of the ligands. There are two ways to model the force field of this zinc ion: the bonded model and the non-bonded model. In the bonded model the coordinates between zinc and ligand/MMP are described by the commonly used bonded terms, including bond stretching.<sup>50–55</sup> On the contrary, in the non-bonded approach, van der Waals and non-bonded electrostatic terms are used to model the zinc–ligand/MMP interactions. The non-bonded method is very sensitive to the choice of electrostatic model and can suffer from an inability to retain a low coordination number. Furthermore, with the AMBER force field, the non-bonded approach generally fails to give the correct coordination number, even when long-range electrostatic interactions are correctly accounted for using an infinite cutoff.<sup>53,56</sup> For all these reasons, we adopted the bonded approach for the zinc ion representation, and therefore specific parameters for the zinc ion had to be added to the AMBER force field.<sup>57</sup> There are many works in the literature regarding the theoretical study of the zinc ion: in 1996, Ryde studied the coordination of the catalytic zinc ion in alcohol dehydrogenase through combined quantum chemical and molecular mechanical calculations,<sup>58</sup> while in 1999 he wrote a theoretical study regarding carboxylate-binding modes.<sup>59</sup> In 2002, Torrent et al. performed an ONIOM study of methane monooxygenase and ribonucleotide reductase,<sup>60</sup> and in 2002 Olsen et al. published a quantum mechanical study concerning the influence of a hydrogen-bonding network on  $\beta$ -lactamase.<sup>61</sup> Regarding MMPs, Donini and Kollman<sup>53</sup> and recently Rizzo et al.<sup>62</sup> carried out, respectively, MM-PBSA and MM-GBSA calculations on certain ligands complexed with MMP-1, MMP-2 and MMP-3, using the zinc non-bonded model. As regards the zinc-bonded model, Toba et al.<sup>56</sup> reported molecular dynamics and free energy perturbation studies carried out on enzyme–inhibitor complexes of human fibroblast collagenases, using AMBER force field parameters coming from

human carbonic anhydrase II studies.<sup>63</sup> These parameters were taken from a tetrahedral model, in which the tetra-coordinated zinc atom was linked with three histidine residues and one water molecule or hydroxide ion; in other cases, the crystal structure of hydroxamate inhibitors complexed with MMPs revealed that the catalytic zinc was penta-coordinated with three histidine nitrogens in MMPs and two hydroxamate oxygens in inhibitors. Consequently, specific force field parameters to study MMPs and their complexes with hydroxamate inhibitors needed to be calculated by quantum mechanical ab initio methods. In this work, we calculated the force field parameters for the structural zinc and the catalytic zinc complexed with hydroxamate inhibitors, and we subsequently tested their efficacy. Furthermore, we studied the docking of some known inhibitors with MMP-1 and -2 and from an analysis of the results, we designed a new MMP-2 active and selective inhibitor.

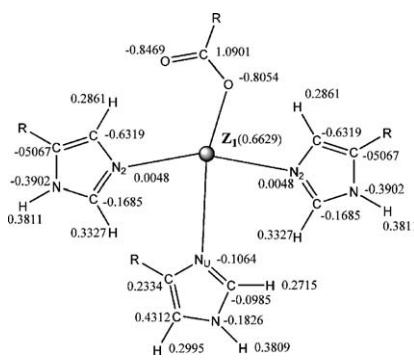
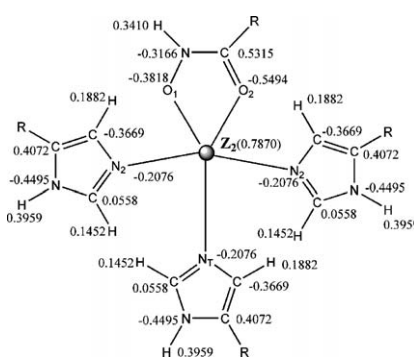
## 2. Results and discussion

### 2.1. Parameter calculations and testing

Starting from the MMP-1 structure derived from experimental crystallographic studies (2TCL),<sup>64</sup> we calculated the geometry, the partial charges and the force constant parameters concerning the two zincs of the metalloproteinases, using the methods reported in Section 4. Table 1 shows all the parameters obtained using this procedure. In order to test the parameters obtained and to verify whether they could be used for molecular dynamics (MD) simulations, we carried out 1 ns of MD on the X-ray structure of MMP-1 (1HFC)<sup>41</sup> complexed with HAP (see Section 4 for details) using our parameters. As shown in Figure 1A, after 140 ps of MD, the system reached an equilibrium, since the total energy for the last 900 ps remained constant. Analyzing the rms deviation from the X-ray structure of all the heavy atoms of the complex, we observed that after an initial increase, in the last 700 ps the rmsd remained approximately constant around the value of 1 Å (see Fig. 1B), suggesting that our MD procedure was correct. As regards the geometry of the sites surrounding the two zincs, during MD we analyzed the rms deviation from the X-ray structure of the position of the two zincs and the heavy atoms of the groups that were bound to the zincs (three imidazoles and the hydroxamic fragment for the catalytic zinc and three imidazoles and the carboxylic fragment for the structural zinc).

As shown in Figure 1C and D, after the first 50 ps of MD, both systems were stabilized with a good rmsd: the average of the rmsd was 0.54 Å for the catalytic zinc binding site and 0.53 Å for the structural one. In order to verify whether using our parameters, the zinc-bonded model gave a better geometry than the zinc non-bonded model, we carried out a second simulation on the MMP-1 X-ray structure, applying the same procedure seen above, but considering the two zincs as non-bonded. Figures 1C and D show that considering the two zinc atoms as non-bonded, the

**Table 1.** Parameters calculated for the structural and catalytic zinc-binding sites

Structural Zn binding site		
		
Interaction	Bond length	Force constant
Z1–N*	2.0766	99.00
Z1–O	2.0192	132.00
Interaction	Angle	Force constant
N*–Z1–N*	111.0000	10.00
C–N*–Z1	126.0000	27.00
C–O–Z1	108.3030	39.00
O–Z1–N2	112.0000	11.55
O–Z1–NU	95.3530	11.55
Catalytic Zn binding site		
		
Interaction	Bond length	Force constant
Z2–N2	2.1051	80.00
Z2–NT	2.1619	70.00
Z2–O1	2.1070	95.00
Z2–O2	2.1111	103.50
O1–N2	1.4061	520.00
Interaction	Angle	Force constant
N2–Z2–N2	111.8620	8.00
N2–Z2–NT	97.9730	8.00
N2–Z2–O2	123.3505	8.75
N2–Z2–O1	90.2945	9.50
NT–Z2–O2	86.7380	8.25
NT–Z2–O1	165.1020	12.85
O1–Z2–O2	78.3650	9.90
C–N*–Z2	126.0000	26.50
N2–O1–Z2	111.8140	67.00
Z2–O2–C	110.5900	33.00

rmsd became worse, exceeding the value of 1 Å in some steps, and in both sites the rmsd average of MD was 0.84 Å. Thus, these results confirmed that the use of the zinc non-bonded model determined a worse geometry of the zinc binding site compared with the one obtained using the bonded model.

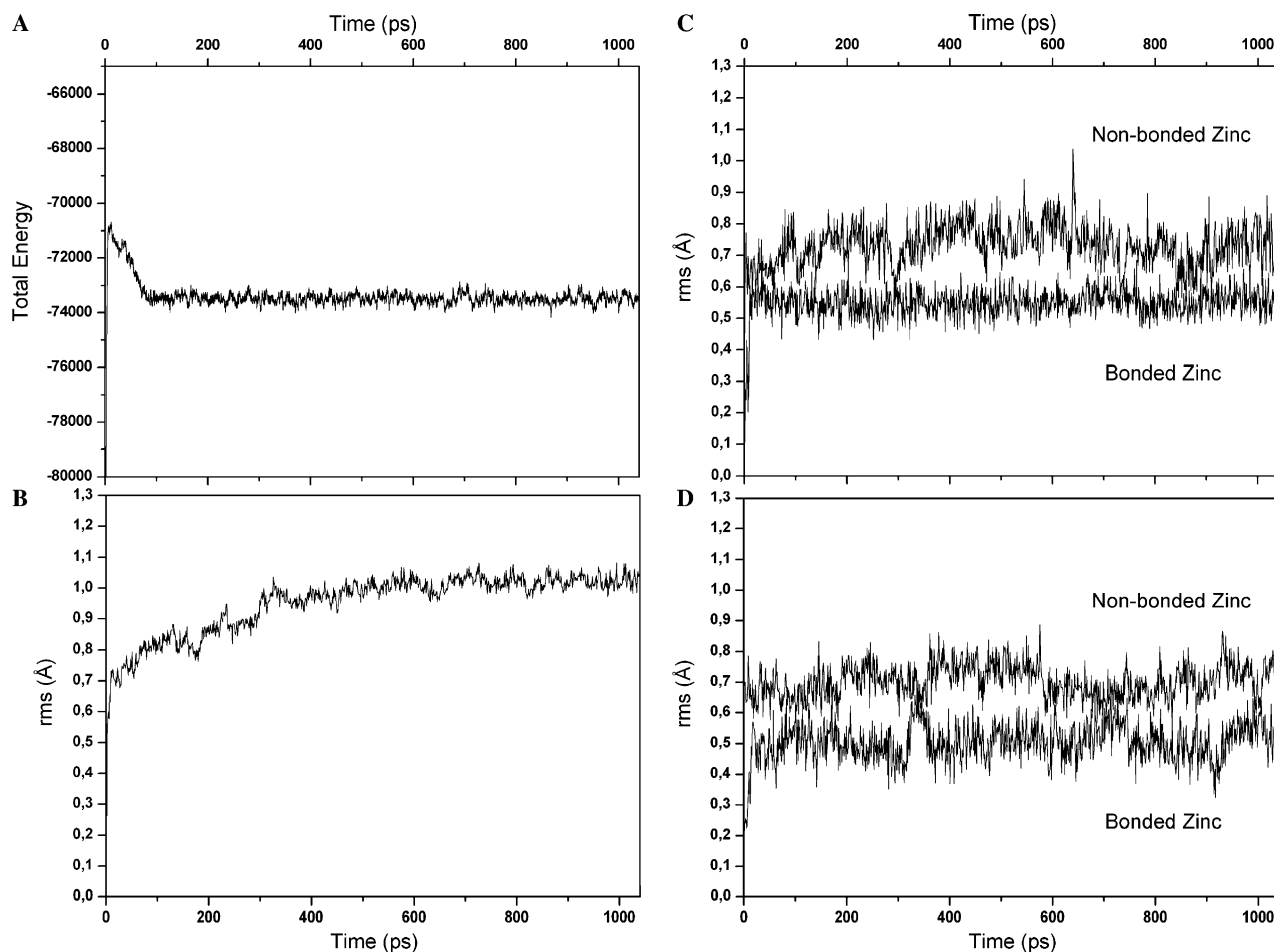


**Figure 1.** Analysis of the MD simulation of HAP complexed with MMP-1. (A) Total energy (kcal/mol) of the system plotted versus time; (B) Root mean square deviation (rmsd) in angstroms (Å) between the system and the X-ray starting structure for all the heavy atoms; (C) rmsd between all the heavy atoms of the catalytic zinc binding site and the X-ray starting structure for the bonded zinc system and non-bonded zinc system; and (D) rmsd between all the heavy atoms of the structural zinc binding site and the X-ray starting structure for the bonded zinc system and non-bonded zinc system.

From the X-ray structure of the complex, we observed that the ligand formed six H bonds with the MMP-1. As shown in Figure 2, HAP interacts with Gly179, Leu181, Ala182, Glu219, Pro238 and Tyr240 (1HFC<sup>41</sup> sequence number). The complex obtained by minimizing the average structure of the last 900 ps of MD showed that all the six H bonds were still present and that the ligand position was very similar to the X-ray one, since the rmsd between the heavy atoms of the ligand was 1.25 Å. Moreover, this value was principally determined by the different position of the phenyl substituent: the rmsd of the heavy atoms of the ligand, excluding those of the phenyl ring, was 0.36 Å (see Fig. 3).

All these analyses proved that the new parameters calculated and our dynamics procedure were reliable and could be used for further docking studies.

## 2.2. Docking studies

We docked Batimastat, CGS 27023A, Prinomastat and compound **a**<sup>48</sup> (see Table 2) into the MMP-1 and MMP-2 using the same procedure described above.

As regards the initial placement of the ligands, the position of Batimastat was very similar to that of HAP, while the other three ligands were introduced inside the binding site in such a manner that they could interact with Leu181, Ala182, Glu219 and with the S1' pocket, in agreement with the experimental data relative to structurally correlated MMP-ligand complexes (see Section 4).

**2.2.1. MMP-1 complexes.** At the end of the simulation, Batimastat presented all the interactions shown by HAP, with the formation of H bonds with Gly179, Leu181, Ala182, Glu219, Pro238 and Tyr240 (see Fig. 5A). The IC<sub>50</sub> values of the two inhibitors confirmed our data as they had a very similar inhibition potency (in MMP-1 HAP showed an IC<sub>50</sub> of 7 nM and Batimastat 10 nM). As regards CGS 27023A, the pyridine substituent interacted in the S2' site, while the isopropyl group was directed towards the His183 of the structural zinc-binding site. The hydroxamate formed H bonds with Ala182 and Glu219, while one of the oxygen atoms of the sulfonamido group interacted with Leu181 and Ala182, forming two H bonds, and



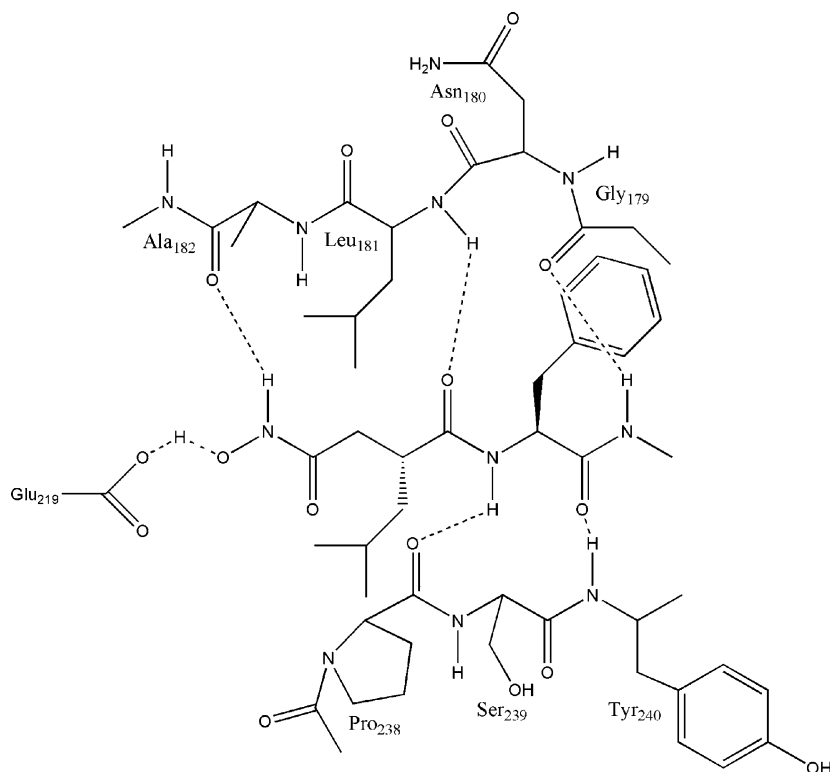


**Figure 2.** Interaction scheme of HAP complexed with MMP-1.

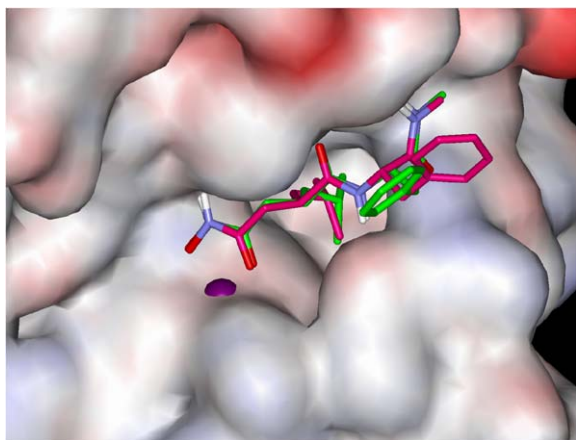


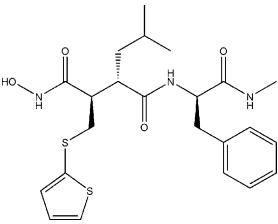
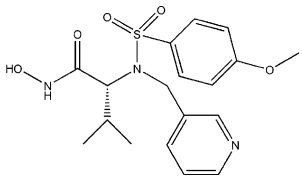
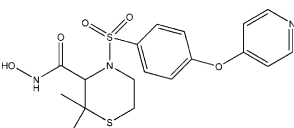
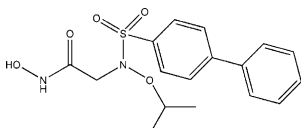
**Figure 3.** Binding position of HAP into MMP-1 after MD compared with the starting X-ray one.

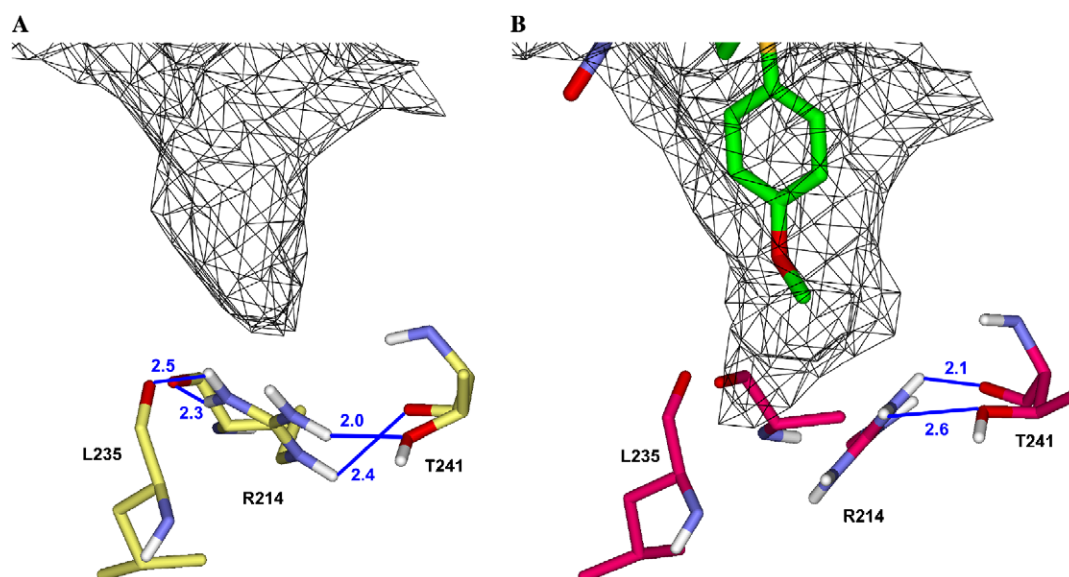
the *p*-methoxyphenyl group was inserted into the S1' pocket (see Fig. 5B). As already known, the MMP-1 S1' pocket is small and closed by the non-conserved residue Arg214 (leucine in MMP-2). Although this residue shows conformational flexibility, it is known that the low inhibition potency of many inhibitors against MMP-1 is often due to the presence of large P1' groups that would require large conformational changes in order to interact with the S1' pocket.<sup>65</sup> Also in our simulation, the presence of the *p*-methoxyphenyl group in the S1' pocket determined a movement of the Arg214: in the initial structure, this residue was stabilized by four H bonds, three of them with Leu235 and Thr241 (two H bonds), and a fourth intramolecular H bond between

the carboxy and amino groups of the same Arg214 (see Fig. 4A); during the simulation, we observed the rotation of the  $\delta$  torsional of the arginine with the disappearance of the intramolecular H bond and the H bond with Leu235, thus determining an increase in the pocket depth (see Fig. 4).

This movement of Arg214 was not observed during the simulation of MMP-1 complexed with Batimastat and HAP, confirming that the conformational adjustment was due to the interaction of the *p*-methoxyphenyl substituent. The position of Prinomastat in MMP-1 was similar to that of CGS 27023A but there were some differences: the hydroxamate formed an H bond with Glu219, losing the interaction with Ala182, and one of the oxygen atoms of the sulfonamido group interacted only with the nitrogen of Leu181, losing the interaction with Ala182 (see Fig. 5C). As regards the S1' pocket, the movement of Arg214 was very similar to that seen in the CGS 27023A-MMP-1 simulation. We observed the rotation of the  $\delta$  torsional of the arginine and the loss of all the H bonds except those with Thr241, but in this complex, the nitrogen of the P1' group of Prinomastat formed an H bond with Thr241. As regards compound **a**, it was unable to penetrate with the P1' substituent inside the S1' pocket completely, thus determining a major solvent exposure of the ligand and low interactions with the MMP-1-binding site, including a bad coordination of the hydroxamate with the zinc atom. As shown in Figure 4D, after about 280 ps of MD, the ligand lost the two H bonds of the oxygen atoms of the sulfonamido chain with Leu181 and Ala182, and only the interaction of the hydroxamate with Glu219

**Table 2.** Ligands used for the docking studies and their MMP-1, -2 inhibitory activity and MMP-1/MMP-2 selectivity

Batimastat		CGS 27023A	
			
		IC <sub>50</sub> (nM) <sup>7</sup>	
MMP-1	MMP-2	MMP-1	MMP-2
10	4	33	20
Ratio	2.5	Ratio	1.7
Prinomastat		Compound a	
			
		IC <sub>50</sub> (nM) <sup>7</sup>	
MMP-1	MMP-2	MMP-1	MMP-2
8	0.08	12460	12.4
Ratio	100	Ratio	1004

**Figure 4.** Analysis of the S1' cavity in the X-ray structure (A) and after modelling with CGS 27023A (B). The presence of the *p*-methoxyphenyl group determines the movement of Arg214 and an increase in cavity depth.

and Ala182 remained. These simulations indicated that Batimastat showed a good inhibition potency, since it presented six H bonds with the protein. CGS 27023A showed four H bonds, but in order to interact in the S1' pocket, the P1' group determined a conformational adjustment of Arg214, with a consequent decrease in inhibition potency. In the MMP-1-Prinomastat complex, we observed the same movement of the arginine, with the formation of a new H bond in the S1' pocket, however, the large

dimensions of the P1' substituent caused its incomplete penetration into the S1' pocket, determining as a consequence the loss of the important interactions with Ala182. Compound **a** proved to be practically inactive in the MMP-1; this was probably due to the presence of the biphenyl group, since this substituent was not able to interact in the S1' pocket, and this fact determined the loss of the interaction of the oxygen atoms of the sulfonamido group with Ala182 and Leu181.

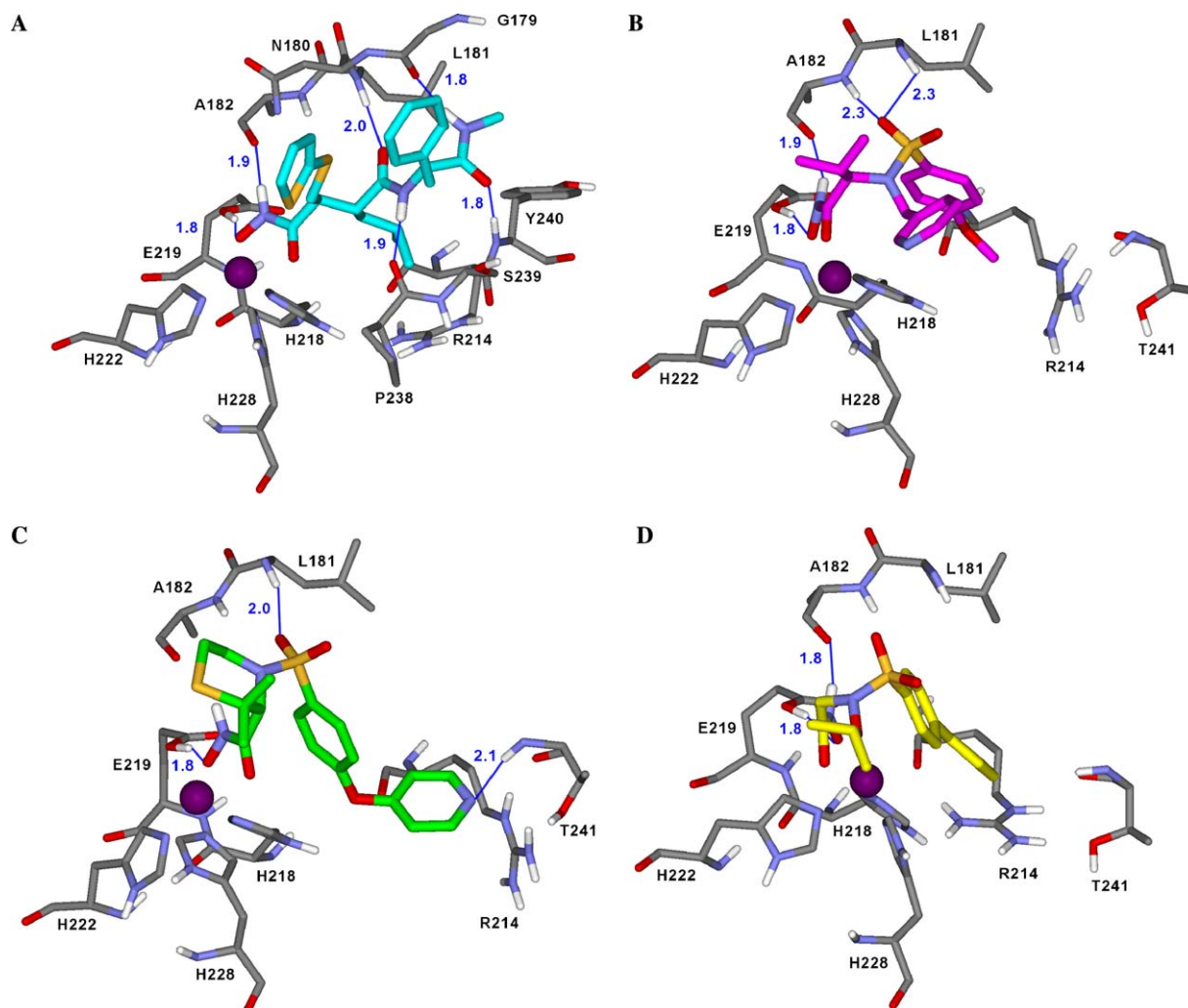


**Figure 5.** Docking of Batimastat (A), CGS 27023A (B), P rinomastat (C) and compound **a** (D) into MMP-1. The main interatomic distances are reported in blue, all distances are in Angstroms.

**2.2.2. MMP-2 complexes.** The docking of Batimastat into MMP-2 showed all the same H bonds that were also present in the MMP-1 complex, thus confirming the low selectivity of this ligand. As in the MMP-1, CGS 27023A showed the pyridine substituent in the S2' site, while the isopropyl group was directed towards the His166 (IQIB<sup>66</sup> sequence number) of the structural zinc-binding site. The hydroxamate formed H bonds with Glu202 and Ala165, while the sulfonamido group interacted with Leu164 and Ala165, forming two H bonds, and the *p*-methoxyphenyl group interacted in the S1' pocket. Prinomastat presented a disposition very similar to that of CGS 27023A: with the hydroxamate it formed two H bonds with Glu202 and Ala165, while the sulfonamido group interacted with Leu164 and Ala165. As regards the P1' substituent, it was inserted into the S1' pocket and formed an H bond with Thr227. Similarly, compound **a** showed the four H bonds with Glu202, Ala165 and Leu164, and the biphenyl system was inserted into the S1' pocket.

**2.2.3. Design of new compounds.** An analysis of the eight complexes suggested that Batimastat showed a good

inhibition potency because of the presence of several H bonds; however, these interactions were maintained in both proteins, and for this reason, this ligand did not show any selectivity. On the contrary, CGS 27023A showed a low level of selectivity, which was probably due to the conformational change that occurred in the MMP-1 pocket to allow the penetration of the *p*-methoxyphenyl group. Prinomastat presented a large P1' substituent, which, although forming two H bonds, determined a conformational adjustment of the ligand in the MMP-1, with the loss of the two crucial interactions with Leu181 and Ala182; this fact could explain its good MMP-2/MMP-1 selectivity. Compound **a** was found to be the most selective ligand of the four analyzed, and this fact could be due to the presence of a large P1' group, rigid and unable to form H bonds, or to interact with the MMP-1-S1' pocket. This analysis suggested that in order to maintain the MMP-2/MMP-1 selectivity, the presence of the biphenyl group as a P1' substituent could be very useful.

In order to improve the MMP-2-inhibitor potency of compound **a**, maintaining its MMP-2/MMP-1 selectivity,

an analysis of the binding site characteristics could be decisive. For this reason, by means of the GRID program,<sup>67</sup> we examined the molecular interaction fields (MIFs) obtained for different probes for the MMP-2. In particular, the examination of the DRY, C1= and C3 probes revealed that besides the lipophilic pocket, corresponding to the S1' pocket, there was a second pocket in which a lipophilic interaction was favourable, and this pocket corresponded to the zone occupied by the CGS 27023A isopropyl group. For this reason, we hypothesized that the design of an analogue of compound **a** with an isopropyl substituent on the alpha carbon atom might be able to increase the MMP-2 inhibition (see Fig. 6), while maintaining a low MMP-1 inhibitory potency, due to the biphenyl group interaction. The substitution of the C alpha determined the formation of a chiral carbon; Figure 7 shows the docking into MMP-2 of the two enantiomers of the designed ligand. In both complexes, the inhibitors formed all the H bonds shown by

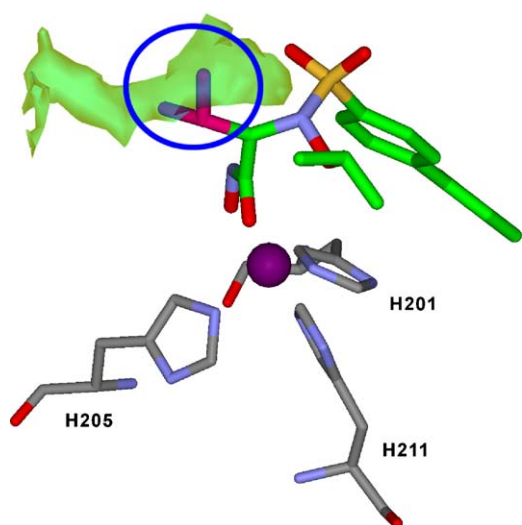


**Figure 6.** GRID analysis of the MMP-2/compound (*R*)-**b** complex. The green surface indicates the lipophilic area highlighted by using the DRY probe; the isopropyl substituent which could interact in this zone is coloured magenta.

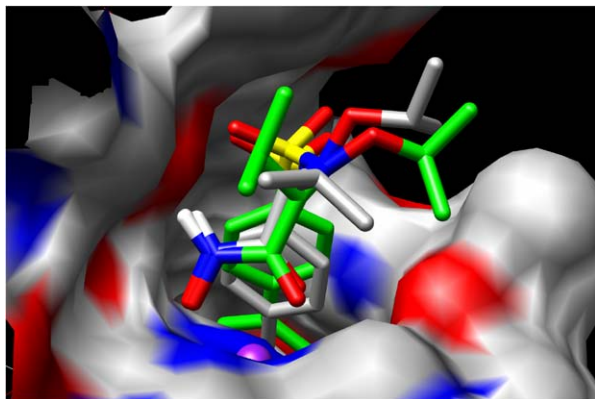


**Figure 7.** Super imposition of (*R*)-**b** (grey) and (*S*)-**b** (green) docked into MMP-2. Unlike (*R*)-**b**, the isopropyl substituent of (*S*)-**b** is directed towards the core of the metalloprotein.

compound **a**, but unlike (*R*)-*N*-hydroxy-2-(*N*-isopropoxybiphenyl-4-ylsulfonamido)-3-methylbutanamide (compound (*R*)-**b**), the *S* enantiomer (compound (*S*)-**b**) presented the isopropyl group directed towards the core of MMP-2, and with this disposition the substituent was unable to interact in the region defined by GRID, leading to worse interactions with the protein.

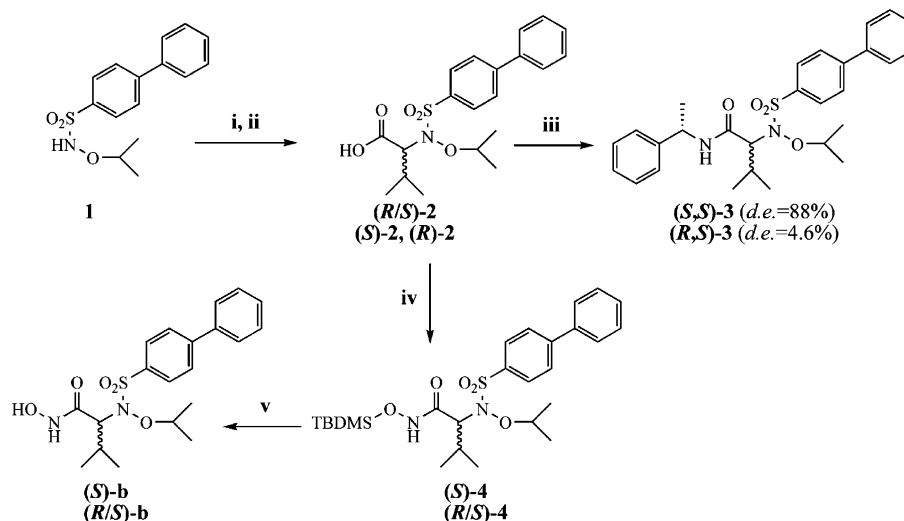
### 2.3. Chemistry

The synthesis of hydroxamates (*S*)-**b** and (*R/S*)-**b** is illustrated in Scheme 1. Intermediate acids (*S*)-**2** and (*R/S*)-**2** were prepared by nucleophilic S<sub>N</sub>2 replacement reaction of the secondary bromides (*R*)- and (*R/S*)-*tert*-butyl 2-bromo-3-methyl butanoate with a caesium salt of the *O*-*i*-propyl-sulfonamide **1**.<sup>48</sup> The same reaction carried out using (*S*)-*tert*-butyl 2-bromo-3-methyl butanoate, in an attempt to obtain the *R* enantiomer of **2**, gave only a poorly enriched enantiomer (*R*)-**2**. The optical purities of these acids ((*S*)-**2** and (*R*)-**2**) were determined by transforming them into their diastereoisomeric amides, (*S,S*)-**3** and (*R,S*)-**3**, by reaction with (*S*)-1-phenylethylamine ((*S*)-PEA).<sup>68</sup> The resulting diastereoisomeric amides, (*S,S*)-**3** and (*R,S*)-**3**, subjected to HPLC analysis to establish their optical purities, gave an acceptable de of 88% only for the amide (*S,S*)-**3**, corresponding to the (*S*)-**2** acid. In the case of the other diastereoisomeric amide, (*R,S*)-**3**, the de was only 4.6%. Consequently only acid (*S*)-**2** was transformed into its hydroxamate (*S*)-**b**. The absolute configuration of (*S*)-**b** was deduced by comparing its optical characteristics with those of an authentic sample of its enantiomer (*R*)-**b**, prepared and optically characterized as described below in Scheme 2.

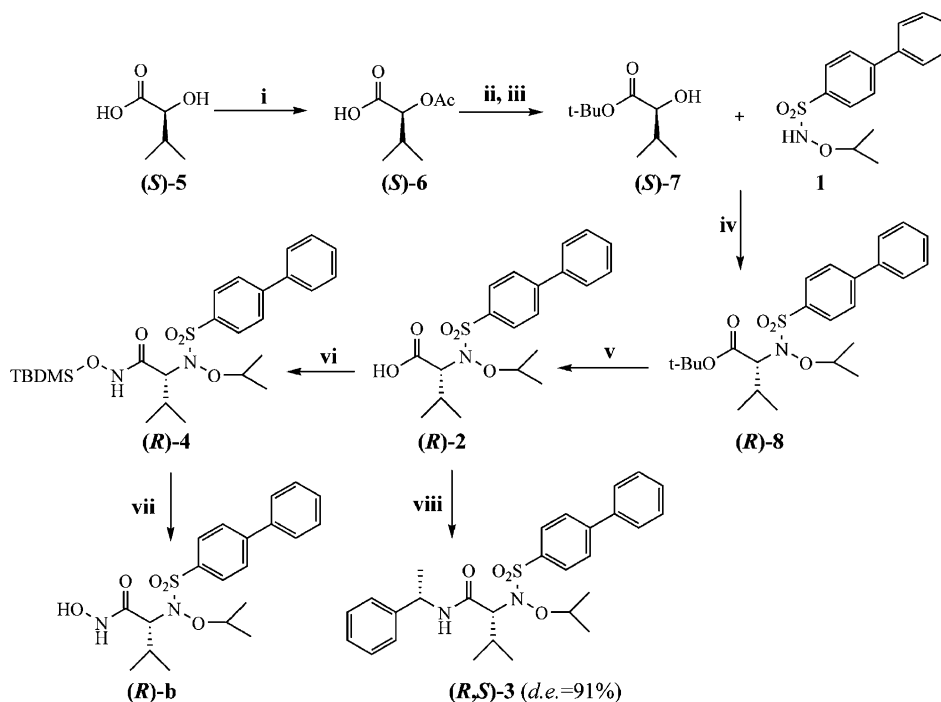
Optically active  $\alpha$ -hydroxy-*tert*-butyl-ester, (*S*)-**7**, was prepared by acetylation of commercial (*S*)-(+)-2-hydroxy-3-methylbutanoic acid (*S*)-**5**, followed by esterification of the stable acetate (*S*)-**6** with *N,N*-dimethylformamide di-*tert*-butyl acetal.<sup>69</sup> A Mitsunobu reaction of sulfonamide **1** with the  $\alpha$ -hydroxy-*tert*-butyl-ester (*S*)-**7** gave the *tert*-butyl ester (*R*)-**8**. Acid cleavage of **8** yielded acid (*R*)-**2**, which was converted to its *O*-silylate (*R*)-**4** and then to the desired hydroxamate (*R*)-**b**. The enantiomeric purity of the hydroxamate (*R*)-**b**, 91%, was determined by NMR spectroscopy using the quinine as chiral solvating agent and based on the splitting of the methine proton of the isopropoxy group of (*R*)-**b** in the equimolecular mixture of (*R*)-**b** with quinine. The (*R*)-absolute configuration of (*R*)-**b** was assigned by analyzing the spatial proximity constraints imposed by NOE measurements carried out on its amide derivative (*R,S*)-**3**, prepared as described above from the enantiopure acid (*R*)-**2**.

**2.3.1. NMR determination of the enantiomeric purity of (*R*)-**b**.** The enantiomeric purity of enantiomerically enriched (*R*)-**b** (16 mM) was determined by NMR spectroscopy (600 MHz, CDCl<sub>3</sub>, 25 °C) by using quinine as the chiral solvating agent<sup>70</sup> and comparing the proton spectrum of the pure compound (*R*)-**b** with those of its equimolar mixture with quinine and of the corresponding mixture containing (*R/S*)-**b**. In particular, the methine proton *b* of the isopropoxy group produced the expected





**Scheme 1.** Reagents and conditions: (i) racemic or (*R*)- or (*S*)-BrCH(*i*Pr)CO<sub>2</sub>*t*Bu, Cs<sub>2</sub>CO<sub>3</sub>, Bu<sub>4</sub>NHSO<sub>4</sub>, DMF, rt, three days; (ii) TFA, CH<sub>2</sub>Cl<sub>2</sub>, 0 °C, 5 h; (iii) (*S*)-1-phenylethylamine, NMM, HOBt, EDCI, CH<sub>2</sub>Cl<sub>2</sub>, rt, 12 h; (iv) TBDMSiONH<sub>2</sub>, EDCI, CH<sub>2</sub>Cl<sub>2</sub>, rt, 18 h; (v) TFA, CH<sub>2</sub>Cl<sub>2</sub>, 0 °C, 5 h.



**Scheme 2.** Reagents and conditions: (i) AcCl, rt, 18 h; (ii) (CH<sub>3</sub>)<sub>2</sub>NCH[OC(CH<sub>3</sub>)<sub>3</sub>]<sub>2</sub>, toluene, 95 °C, 3 h; (iii) LiOH, THF/MeOH/H<sub>2</sub>O, rt, 3 h; (iv) PPh<sub>3</sub>, DEAD, THF, 0 °C, 5 h; (v) TFA, CH<sub>2</sub>Cl<sub>2</sub>, 0 °C, 5 h; (vi) TBDMSiONH<sub>2</sub>, EDCI, CH<sub>2</sub>Cl<sub>2</sub>, rt, 18 h; (vii) TFA, CH<sub>2</sub>Cl<sub>2</sub>, 0 °C, 5 h; (viii) (*S*)-1-phenylethylamine, NMM, HOBt, EDCI, CH<sub>2</sub>Cl<sub>2</sub>, rt, 12 h.

multiplet at 4.46 ppm. In the mixture containing (*R/S*)-**b** and quinine, the same signal was split into two resonances centred at 4.45 and 4.47 ppm having equal intensities. In the mixture containing enriched (*R*)-**b**, only small amounts of the signal at 4.45 ppm were detected, allowing us to calculate an enantiomeric purity of 91%.

**2.3.2. NMR determination of the absolute configuration of (*R*)-b.** The (*R*)-absolute configuration of (*R*)-**b** was assigned by analyzing the spatial proximity constraints

imposed by NOE measurements carried out on its diastereoisomeric pure amide derivative (*R,S*)-**3**. The <sup>1</sup>H NMR (600 MHz, CDCl<sub>3</sub>, 25 °C) spectrum of (*R,S*)-**3** (see Fig. 8) shows signals going from 0.6 to 8.2 ppm. The low frequency region (0.6–2.2 ppm) included methyl protons and the methine proton H<sub>d</sub>. In the spectral region going from 3.7 to 6.6 ppm, three well-separated broad resonances were detected: a singlet at 3.88 ppm generated by H<sub>c</sub>, a singlet (2H) at 4.50 ppm due to the superimposition of H<sub>b</sub> and H<sub>n</sub> resonances, and a singlet

at 6.43 ppm produced by the amide proton  $\text{NH}_m$ . The aromatic nuclei resonances were found in the high frequency region.

In the ROESY trace corresponding to the methine proton  $c$ , three similar interNOEs  $\text{H}_c\text{--NH}_m$ ,  $\text{H}_c\text{--H}_d$  and  $\text{H}_c\text{--H}_f$  were detected, allowing us to state the cisoid arrangement between them. Accordingly, the amide proton  $\text{NH}_m$  produced intense interNOEs with  $\text{H}_c$  and  $\text{H}_d$  and a weaker one with the aromatic protons  $\text{H}_f$ . The methyl group of the 1-phenylethyl moiety originated a dipolar interaction with the methine proton  $\text{H}_d$  (see Fig. 9).

On the basis of the above-discussed NOE data, the stereochemistry of the molecule was defined, with the  $\text{N--H}_m$  and  $\text{C--H}_c$  bonds cisoid and in close proximity of the aromatic biphenyl moiety, and the methyl protons  $\text{H}_o$  bent at  $\text{H}_d$ , which was close to  $\text{H}_c$ . Even if these proximity constraints can be satisfied by both diastereoisomers  $R,S$  and  $S,S$ , the presence of interNOEs  $\text{H}_f\text{--Ph}$ , which means that the two aromatic rings face each

other, can be justified only in the case of the  $R$ -absolute configuration of the chiral carbon  $c$ .

## 2.4. Biological results

Table 3 shows the inhibitory indices ( $\text{IC}_{50}$ ) towards MMP-1 and MMP-2 of the  $N$ -hydroxy-2-( $N$ -isopropoxybiphenyl-4-ylsulfonamido)-3-methylbutanamides (( $R,S$ )-**b**, ( $R$ )-**b** and ( $S$ )-**b**), compared with those of the previously described  $N$ -hydroxy-2-( $N$ -isopropoxybiphenyl-4-ylsulfonamido)acetamide (compound **a**). Selectivity indices for MMP-2 over MMP-1, are expressed as ratios of their inhibitory indices. On MMP-2, the substitution on the P1 site with an  $i$ -Pr group on the carbon atom alpha to the hydroxamate improves the inhibitory potency about five times, passing from compound **a** ( $\text{IC}_{50} = 12.4$  nM) to racemic ( $R,S$ )-**b** ( $\text{IC}_{50} = 2.44$  nM). The ( $R$ )-**b** enantiomer shows an improvement of the potency on MMP-2 of threefold ( $\text{IC}_{50} = 0.81$  nM) compared with its racemate ( $R,S$ )-**b** and about nineteen times, compared with its dystomer ( $S$ )-**b** ( $\text{IC}_{50} = 15.2$  nM). In agreement with the previous studies of the British Biotech company.<sup>88</sup> An analysis of the selectivity indices for the  $N$ -hydroxy-2-( $N$ -isopropoxybiphenyl-4-ylsulfonamido)-3-methylbutanamides (( $R,S$ )-**b**, ( $R$ )-**b** and ( $S$ )-**b**) and the alpha unsubstituted compound  $N$ -hydroxy-2-( $N$ -isopropoxybiphenyl-4-ylsulfonamido)acetamide (compound **a**)

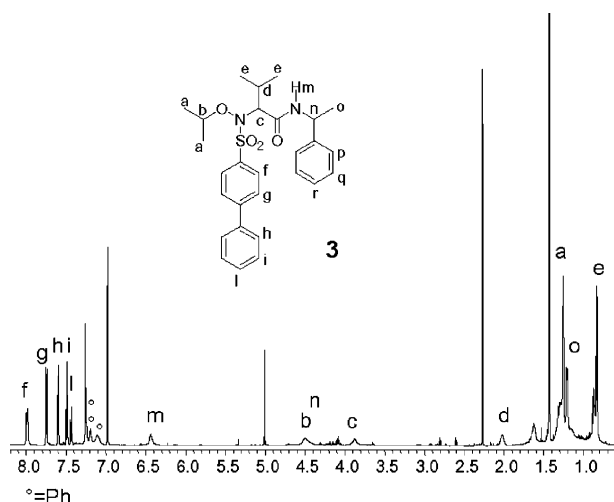


Figure 8.  $^1\text{H}$  NMR (600 MHz,  $\text{CDCl}_3$ , 25 °C) spectrum of **3**.

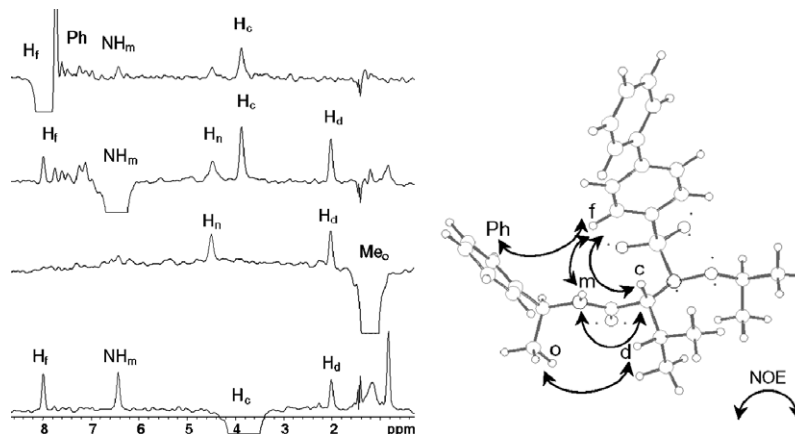


Figure 9. ROESY traces (600 MHz,  $\text{CDCl}_3$ , mix 0.3 s) and stereochemical representation of spectrum of **3**.

Table 3. Inhibitory activity of  $N$ -hydroxy-2-( $N$ -isopropoxybiphenyl-4-ylsulfonamido)acetamide (compound **a**) and  $N$ -hydroxy-2-( $N$ -isopropoxybiphenyl-4-ylsulfonamido)-3-methylbutanamides (( $R,S$ )-**b**, ( $R$ )-**b** and ( $S$ )-**b**) towards MMP-1 and MMP-2

Compound	$\text{IC}_{50}$ (nM)		
	MMP-1 <sup>a</sup>	MMP-2 <sup>a</sup>	MMP-1/MMP-2 ratio <sup>b</sup>
<b>a</b>	12,460 ± 960	12.4 ± 1.5	1004.9
( $R,S$ )- <b>b</b>	590 ± 25	2.44 ± 0.28	241.8
( $R$ )- <b>b</b>	486 ± 76	0.81 ± 0.22	600
( $S$ )- <b>b</b>	1199 ± 52	15.2 ± 1.3	78.9

<sup>a</sup> Mca-Lys-Pro-Leu-Gly-Leu-Dap (Dnp)-Ala-Arg- $\text{NH}_2$  and Mca-Pro-Leu-Gly-Leu-Dpa-Ala-Arg- $\text{NH}_2$  have been used as substrates for MMP-1 and MMP-2, respectively.

<sup>b</sup> Selectivity indices are reported as MMP-1/MMP-2  $\text{IC}_{50}$  ratios.

indicates that the newly synthesized P1 substituted (*i*-Pr group) compounds maintain a good selectivity profile. As can be seen, the MMP-1/MMP-2 ratios range from 241.8 for the racemic (*R/S*)-**b** to 600 for the eutomer (*R*)-**b**, respectively. A comparison of these selectivity indices with that of the previous *N*-hydroxy-2-(*N*-isopropoxybiphenyl-4-ylsulfonamido)acetamide (compound **a**) indicates a reduction of about two times of the selectivity ratio MMP-1/MMP-2 passing from the new, most potent MMP-2 inhibitor, (*R*)-**b** to compound **a**. In every case, a comparison between the new in vitro potent antiangiogenic agent MMP-2 inhibitor (*R*)-**b**<sup>1</sup> and the reference drugs used indicates that this compound is 24.7 times more potent on MMP-2 than the reference drug CGS 27023A. Moreover (*R*)-**b** proves to be 352.9 and 6 times more selective than CGS 27023A and Prinomastat, respectively.

### 3. Conclusions

In a rational planning of the new biphenylsulfonamido-based hydroxamate derivatives recently studied by us, which possess a good selectivity for MMP-2 over MMP-1, we obtained the parameters for studying MMPs and their complexes with hydroxamate inhibitors by means of the AMBER force field. This modified force field was able to simulate the geometrical data derived from X-ray structures, thus making it possible to carry out reliable molecular modelling studies on hydroxamate inhibitor-MMP complexes. On the basis of the docking studies, the two enantiomers of *N*-hydroxy-2-(*N*-isopropoxybiphenyl-4-ylsulfonamido)-3-methylbutanamide, (*R*)-**b** and (*S*)-**b**, were designed and synthesized, as more potent MMP-2 inhibitors than our previous compound **a**. An analysis of the inhibition profile on MMP-1 and MMP-2 of these two inhibitors shows that the eutomer (*R*)-**b** is 24.7 times and 15.3 times more potent than CGS 27023A and the parent compound **a** on MMP-2, maintaining a higher index of MMP-2/MMP-1 selectivity compared with the CGS 27023A and Prinomastat.

On this basis, the hydroxamate (*R*)-**b** can be considered as a progenitor of a new class of biphenylsulfonamido-based inhibitors that differ from **a** in the presence of an alkyl side chain in the P1' position and show a good potency and selectivity profile on the two MMPs studied.

### 4. Experimental

#### 4.1. Parameter calculations

In order to obtain all the parameters regarding the structural and catalytic zinc, it was necessary to optimize the geometry of the two systems, calculate the partial charges and then estimate and optimize the missing Force constants.

**4.1.1. Geometry optimization.** Starting from the geometry arising from the experimental crystallographic

structure of MMP-1,<sup>64</sup> we constructed two models referring to the two zinc ions with their chemical surroundings. The model referring to the structural zinc was made up of three methylimidazoles and one acetate ion, while the one referring to the catalytic zinc was made up of three methylimidazoles and one acetylhydroxamate ion (see figures of Table 1 where R is replaced by methyl). These models were subjected to a full geometry optimization by means of quantum mechanical calculations based on the Gaussian98 program,<sup>71</sup> using the B3LYP chemical model with a LanL2DZ basis set, a direct SCF calculation and an SCF convergence criterion to 10<sup>−5</sup>. The B3LYP chemical model has been shown to be an accurate density functional method,<sup>72</sup> and it gives as good or better geometries and energies as MP2 ab initio methods for first-row transition metal complexes.<sup>73</sup> The B3LYP model is a combination of the Becke three-parameter hybrid functional<sup>74</sup> with the Lee–Yang–Parr correlation functional (which also includes density gradient terms).<sup>75,76</sup> As regards the basis set, we used LanL2DZ; this means that the zinc atom is described through the Los Alamos non-relativistic electron core potential of Hay and Wadt<sup>77</sup> and an essentially double-zeta basis set including 3d orbitals and 3d diffuse functions for the valence shell. In this basis set, the rest of the atoms are described through the Dunning–Huzinaga full double- $\zeta$  basis set.<sup>78</sup> This method has already been tested and has been found to be suitable to deal with systems containing metal atoms, and in particular zinc.<sup>60,79</sup>

**4.1.2. Partial charges.** The next step was to determine the charges to be assigned to the zinc, to its chemical surroundings, and, lastly, to the ligands. The method used was an analysis of the RESP<sup>80</sup> (restrained electrostatic potential fit); the basic idea behind this charge-fitting algorithm is that the charges on non-hydrogen atoms are restrained to an ‘optimal’ value of zero. The RESP charges show less conformational variability than the standard ESP charges.

**4.1.3. Force constants.** A frequency analysis was carried out on the two models, and the diagonal elements of the Hessian matrix, calculated in their internal coordinates, were used as the value of the stretching constants. The bending force constants were approximated to one-tenth of the relative stretching constants. The torsional force constants for zinc were not taken into consideration, since the geometry refers to a structure which is quite rigid and devoid of any significant torsional freedom.<sup>63</sup> Given that molecular mechanics not only takes into consideration the binding terms, but also the non-binding ones (Coulombian and van der Waals interactions), unlike quantum mechanics which determines the total energy, it was necessary to test the values of the force constants, obtained by means of frequency calculations, within the AMBER force field, and, where necessary, to adjust these values. For this reason, several conformations were taken into consideration, in which the stretching and bending values were varied around the equilibrium value. Quantum mechanical calculations were carried out on these models by the B3LYP/LanL2DZ method, together with energy calculations

based on the AMBER force field with the parameters calculated for the zinc ion. Only small adjustments were required to the force constants obtained from the frequency calculation, in order to obtain the best agreement between the energy values calculated by the two methods. In fact, the modified AMBER force field after optimization was able to calculate the conformational energy of the model with a very good agreement with respect to the DFT-B3LYP-LanL2DZ method and, for the different parameters, the rms of the difference between the relative energies (kilocalories per mole) calculated by means of quantum mechanics (B3LYP/LanL2DZ) and those calculated by means of molecular mechanics (AMBER) showed an average value of 0.85 Å.

#### 4.2. MD simulations

All simulations were performed using AMBER 8.0.<sup>81</sup> MD simulations were carried out using the modified parm94 force field at 300 K. An explicit solvent model TIP3P water was used and the complexes were solvated with a 15 Å water cap. Sodium ions were added as counterions to neutralize the system. Prior to MD simulations, two steps of minimization were carried out; in the first stage, we kept the protein fixed with a constraint of 500 kcal/mol and we just minimized the positions of the water molecules; then in the second stage, we minimized the entire system applying a constraint of 20 kcal/mol on the  $\alpha$  carbon. The two minimization stages consisted of 5000 steps in which the first 1000 were steepest descent (SD) and the last 4000 conjugate gradient (CG). Molecular dynamics trajectories were run using the minimized structure as a starting input, and the particle mesh Ewald (PME) algorithm was used for dealing with long-range interactions.<sup>82</sup> The time step of the simulations was 2.0 fs with a cutoff of 12 Å for the non-bonded interaction and SHAKE was employed to keep all bonds involving hydrogen atoms rigid. Constant-volume was carried out for 40 ps, during which the temperature was raised from 0 to 300 K (using the Langevin dynamics method); then 600 ps (1 ns for the X-ray complex) of constant-pressure MD was carried out at 300 K. All the  $\alpha$  carbons not within 15 Å of the catalytic zinc were blocked with a harmonic force constant of 20 kcal/mol Å. The final structure of the complexes was obtained as the average of the last 500 ps of MD minimized with the CG method until a convergence of 0.05 kcal/mol Å.

#### 4.3. Docking of the ligands

The four inhibitors were placed into MMP-1 (1HFC)<sup>41</sup> and MMP-2 (1QIB)<sup>66</sup> using as reference positions those of the MMP complexes determined by X-ray and NMR methods deposited at the Protein Databank.<sup>83</sup> For Batimastat, we superimposed the binding site of MMP-1 and MMP-2 on the MMP-8-Batimastat complex (1MMB).<sup>84</sup> As regards Prinomastat, we used the position of a diphenyl-ether sulfone-based hydroxamic acid complexed with the MMP-1 (966C)<sup>65</sup> as a template, while for CGS 27023A and compound **a** we used the

NMR study carried out on MMP-2 complexed with a hydroxamic acid inhibitor (1HOV).<sup>85</sup>

#### 4.4. GRID calculations

The GRID box dimensions were chosen to encompass all the important parts of the active site. The grid spacing was set to 1 Å, and the molecular interaction fields (MIFs) were calculated for the DRY (hydrophobic probe), C1= (sp<sup>2</sup> CH aromatic or vinyl), C3 (methyl CH<sub>3</sub> group), N2 (neutral flat NH<sub>2</sub>, e.g., amide), O (sp<sup>2</sup> carbonyl oxygen) and OH (phenol or carboxy OH) probes using the GRID program, version 22.<sup>67</sup>

#### 4.5. General synthetic methods and materials

All commercially available starting materials and solvents were of reagent grade. Solutions containing products were dried over anhydrous sodium sulfate (Na<sub>2</sub>SO<sub>4</sub>). Melting points were determined on a Kofler hot-stage apparatus and are uncorrected. <sup>1</sup>H NMR spectra were recorded on a Varian Gemini 200 (200 MHz) or a Varian INOVA600 spectrometer operating at 600 MHz using a 5 mm broadband inverse probe with z-axis gradient, and CDCl<sub>3</sub> or DMSO-*d*<sub>6</sub> as solvents unless otherwise indicated. Peak positions are given in parts per million (ppm,  $\delta$  units). Mass spectra were recorded on a GC/MS Trace GCQ Plus Thermo Quest Finnigan spectrometer using a direct injection probe and an electron beam energy of 40 eV. Optical rotations were obtained on a Perkin-Elmer 241 polarimeter with a continuous Na lamp (569 nm). Reactions were routinely monitored by thin-layer chromatography (TLC) on 0.25 mm silica gel plates (Merck 60 F<sub>254</sub>) and hydroxamic acids were visualised with FeCl<sub>3</sub> aqueous solution. Flash chromatography was carried out through glass columns containing silica gel 60 (Merck 230–400 Mesh). HPLC analysis was carried out with a liquid Waters Associates chromatograph 6000 A, equipped with a 480 UV detector reading at 254 nm, using a Resolver Spherical C<sub>18</sub> (Merck 3.9 × 300 mm) 5  $\mu$ m column. Elemental analyses were carried out by our analytical laboratory and were consistent with theoretical values to within  $\pm 0.4\%$ .

**4.5.1. General procedure for the preparation of carboxylic acids (R/S)-2, (S)-2 and (R)-2.** A solution of the sulfonamide **1** (1 mmol) in anhydrous DMF (3 mL) was treated with racemic, (R) or (S)-*tert*-butyl 2-bromo-3-methyl butanoate (1.2 mmol), caesium carbonate (1 mmol) and tetrabutylammonium hydrogen sulfate (1 mmol). The reaction mixture was stirred for 3 days at room temperature, diluted with H<sub>2</sub>O (3 × 20 mL) and extracted three times with EtOAc (20 mL) giving, after work-up, racemic, (S)- and (R)-*tert*-butyl esters which were used in the next step without further purification. TFA (4.4 mL, 57 mmol) was added dropwise to a stirred, ice-chilled solution of racemic, (S)- and (R)-*tert*-butyl esters (1 mmol) in freshly distilled (P<sub>2</sub>O<sub>5</sub>) dichloromethane (3.4 mL). The mixture was stirred under these reaction conditions for 5 h and the solvent was removed in vacuo to give the carboxylic acids (R/S)-2, (S)-2 or (R)-2.



**4.5.2. (*R/S*)-2-(*N*-Isopropoxybiphenyl-4-ylsulfonamido)-3-methylbutanoic acid (*R/S*)-2.** The title compound was prepared from ( $\pm$ )-*tert*-butyl 2-bromo-3-methyl butanoate following the general procedure. White solid (60.3% yield); mp 156–158 °C;  $^1\text{H}$  NMR ( $\text{CDCl}_3$ )  $\delta$ : 0.87 (d,  $J$  = 6.4 Hz, 6H); 1.21 (d,  $J$  = 6.2 Hz, 3H); 1.27 (d,  $J$  = 6.2 Hz, 3H); 2.12 (m, 1H); 3.84 (d,  $J$  = 10.0 Hz, 1H); 4.44 (septet,  $J$  = 6.2 Hz, 1H); 7.42–7.51 (m, 3H); 7.59–7.62 (m, 2H); 7.66–7.70 (m, 2H); 7.90–7.94 (m, 2H). Anal. Calcd for  $\text{C}_{20}\text{H}_{25}\text{NO}_5\text{S}$ : C, 61.36; H, 6.44; N, 3.58. Found: C, 61.50; H, 6.55; N, 3.50.

**4.5.3. (*S*)-2-(*N*-Isopropoxybiphenyl-4-ylsulfonamido)-3-methylbutanoic acid (*S*)-2.** The title compound was prepared from (*R*)-*tert*-butyl 2-bromo-3-methyl butanoate following the general procedure. White solid (94.4% yield); mp 159–161 °C;  $[\alpha]_{\text{D}}^{20}$  –88.35 ( $c$  0.01, MeOH);  $^1\text{H}$  NMR ( $\text{CDCl}_3$ )  $\delta$ : 0.91 (d,  $J$  = 6.5 Hz, 6H); 1.25 (d,  $J$  = 6.2 Hz, 3H); 1.30 (d,  $J$  = 6.2 Hz, 3H); 2.13 (m, 1H); 3.90 (d,  $J$  = 10.4 Hz, 1H); 4.48 (septet,  $J$  = 6.2 Hz, 1H); 7.42–7.53 (m, 3H); 7.59–7.64 (m, 2H); 7.68–7.72 (m, 2H); 7.91–7.95 (m, 2H). Anal. Calcd for  $\text{C}_{20}\text{H}_{25}\text{NO}_5\text{S}$ : C, 61.36; H, 6.44; N, 3.58. Found: C, 61.42; H, 6.46; N, 3.57.

**4.5.4. (*R*)-2-(*N*-Isopropoxybiphenyl-4-ylsulfonamido)-3-methylbutanoic acid (*R*)-2.** The title compound was prepared from (*S*)-*tert*-butyl 2-bromo-3-methyl butanoate following the general procedure. White solid (71% yield); mp 135–137 °C;  $[\alpha]_{\text{D}}^{20}$  +6 ( $c$  0.01, MeOH);  $^1\text{H}$  NMR ( $\text{CDCl}_3$ )  $\delta$ : 0.91 (d,  $J$  = 6.4 Hz, 6H); 1.24 (d,  $J$  = 6.2 Hz, 3H); 1.31 (d,  $J$  = 6.2 Hz, 3H); 2.12 (m, 1H); 3.90 (d,  $J$  = 10.2 Hz, 1H); 4.48 (septet,  $J$  = 6.2 Hz, 1H); 7.42–7.53 (m, 3H); 7.59–7.64 (m, 2H); 7.68–7.72 (m, 2H); 7.91–7.95 (m, 2H). Anal. Calcd for  $\text{C}_{20}\text{H}_{25}\text{NO}_5\text{S}$ : C, 61.36; H, 6.44; N, 3.58. Found: C, 61.47; H, 6.45; N, 3.57.

**4.5.5. Preparation of diastereoisomeric amides (*S,S*)-3 and (*R,S*)-3 from acid (*R/S*)-2.** To a solution of the carboxylic acid (*R/S*)-2, (56.5 mg, 0.14 mmol) in freshly distilled ( $\text{P}_2\text{O}_5$ )  $\text{CH}_2\text{Cl}_2$  (2.2 mL) were added (*S*)-1-phenylethylamine (0.018 mL, 0.14 mmol), NMM (0.030 mL, 0.28 mmol), HOBt (18.9 mg, 0.14 mmol) and EDCI (26.8 mg, 0.14 mmol). The reaction mixture was stirred overnight at room temperature. The organic layer, washed with water and brine, dried over anhydrous  $\text{Na}_2\text{SO}_4$  and evaporated at reduced pressure, gave an oil consisting of a 1:1 diastereoisomeric mixture of amides (*R,S*)-3 and (*S,S*)-3 ( $^1\text{H}$  NMR, HPLC). The crude oil was purified by column chromatography on silica gel, eluting with a mixture of isopropyl ether/TEA, 98:2. The first fractions obtained gave pure (*R*)-2-(*N*-isopropoxybiphenyl-4-ylsulfonamido)-3-methyl-*N*-((*S*)-1-phenylethyl)butanamide (**3**) as an oil.  $^1\text{H}$  NMR ( $\text{CDCl}_3$ )  $\delta$ : 0.83 (d,  $J$  = 6.6 Hz, 6H); 1.21 (d,  $J$  = 6.2 Hz, 3H); 1.23–1.27 (m, 2H); 2.01 (m, 1H); 3.86 (m, 1H); 4.40–4.60 (m, 2H); 6.44 (m, 1H); 7.13–7.22 (m, 5H); 7.42–7.54 (m, 3H); 7.57–7.63 (m, 2H); 7.73–7.77 (m, 2H); 7.97–8.01 (m, 2H). Anal. Calcd for  $\text{C}_{28}\text{H}_{34}\text{N}_2\text{O}_4\text{S}$ : C, 67.99; H, 6.93; N, 5.66. Found: C, 68.09; H, 6.93; N, 5.46. HPLC:  $t_{\text{R}}$  = 51.2 min  $F$  = 0.5  $\mu\text{L}/\text{min}$ ; eluent: MeOH/ $\text{H}_2\text{O}$ , 73:27. From the

second fractions, pure (*S*)-2-(*N*-isopropoxybiphenyl-4-ylsulfonamido)-3-methyl-*N*-((*S*)-1-phenylethyl)butanamide (**3**) was obtained as an oil.  $^1\text{H}$  NMR ( $\text{CDCl}_3$ )  $\delta$ : 0.95 (d,  $J$  = 6.5 Hz, 6H); 1.12 (m, 9H); 2.08 (m, 1H); 3.82 (d,  $J$  = 9.4 Hz, 1H); 4.46–4.58 (m, 2H); 6.40 (d,  $J$  = 7.1 Hz, 1H); 7.02–7.25 (m, 5H); 7.42–7.55 (m, 7H); 7.86–7.90 (m, 2H). Anal. Calcd for  $\text{C}_{28}\text{H}_{34}\text{N}_2\text{O}_4\text{S}$ : C, 67.99; H, 6.93; N, 5.66. Found: C, 68.03; H, 6.94; N, 5.60. HPLC:  $t_{\text{R}}$  = 52.8 min;  $F$  = 0.5  $\mu\text{L}/\text{min}$ ; eluent: MeOH/ $\text{H}_2\text{O}$ , 73:27.

**4.5.6. General procedure for the preparation of diastereoisomeric amides (*S,S*)-3 and (*R,S*)-3 from optically enriched acids (*S*)-2 and (*R*)-2.** The title diastereoisomers were obtained from acids (*S*)-2 and (*R*)-2 according to the synthetic method described above. HPLC analysis carried out as described above on both the crude reaction mixtures, in order to determine their de, gave the following results:

(*S,S*)-3. HPLC: (*R,S*) amide:  $t_{\text{R}}$  = 50.9 min (6%); (*S,S*) amide:  $t_{\text{R}}$  = 52.7 min (94%), de 88%.

(*R,S*)-3. HPLC: (*R,S*) amide:  $t_{\text{R}}$  = 51.2 min (52.3%); (*S,S*) amide:  $t_{\text{R}}$  = 52.9 min (47.7%), de 4.6%.

**4.5.7. General procedure for the preparation of *O*-TBDMS acid hydroxyamides (*S*)-4 and (*R/S*)-4.** 1-[3-(Dimethylamino)propyl]-3-ethyl carbodiimide hydrochloride (EDCI) was added portionwise (1 mmol) to a stirred and cooled solution (0 °C) of the carboxylic acid (*S*)-2 or (*R/S*)-2 (1 mmol), and *O*-(*tert*-butyldimethylsilyl)hydroxylamine (1 mmol) in freshly distilled ( $\text{P}_2\text{O}_5$ )  $\text{CH}_2\text{Cl}_2$  (18 mL). After stirring at room temperature for 24 h, the mixture was washed with water (20 mL) and the organic phase was dried and evaporated in vacuo. The crude residue was purified by flash chromatography on silica gel to yield (*S*)-4 and (*R/S*)-4 as oils.

**4.5.8. (*S*)-*N*-(*tert*-Butyldimethylsilyloxy)-2-(*N*-isopropoxybiphenyl-4-ylsulfonamido)-3-methylbutanamide (*S*)-4.** The title compound was prepared from the carboxylic acid (*S*)-2 following the general procedure. The crude product was purified by flash chromatography on silica gel (*n*-hexane/EtOAc, 4:1) to yield (*S*)-4 (27.4% yield) as an oil.  $R_{\text{f}}$  = 0.25;  $^1\text{H}$  NMR ( $\text{CDCl}_3$ )  $\delta$ : 0.06 (s, 6H); 0.84–0.94 (m, 15H); 1.24–1.29 (m, 6H); 2.14 (m, 1H); 3.81 (m, 1H); 4.39 (m, 1H); 7.41–7.51 (m, 3H); 7.61–7.64 (m, 2H); 7.75–7.79 (m, 2H); 7.95–7.98 (m, 2H); 8.17 (br s, 1H). Anal. Calcd for  $\text{C}_{26}\text{H}_{40}\text{N}_2\text{O}_5\text{Si}$ : C, 59.97; H, 7.74; N, 5.38. Found: C, 60.02; H, 7.75; N, 5.36.

**4.5.9. (*R/S*)-*N*-(*tert*-Butyldimethylsilyloxy)-2-(*N*-isopropoxybiphenyl-4-ylsulfonamido)-3-methylbutanamide (*R/S*)-4.** The title compound was prepared from the racemic carboxylic acid (*R/S*)-2 following the general procedure. The crude product was purified by flash chromatography on silica gel (*n*-hexane/EtOAc, 4:1) to give (*R/S*)-4 (30% yield) as a yellow oil.  $^1\text{H}$  NMR ( $\text{CDCl}_3$ )  $\delta$ : 0.06 (s, 6H); 0.84–0.94 (m, 15H); 1.24–1.27 (m, 6H); 2.14 (m, 1H); 3.82 (m, 1H); 4.39 (m, 1H); 7.41–7.52 (m, 3H); 7.60–7.65 (m, 2H); 7.74–7.79 (m, 2H); 7.94–7.98 (m, 2H); 8.17 (br s, 1H). Anal. Calcd

for  $C_{26}H_{40}N_2O_5SSi$ : C, 59.97; H, 7.74; N, 5.38. Found: C, 60.05; H, 7.75; N, 5.37.

**4.5.10. General procedure for the preparation of acid hydroxyamides (S)-(b) and (R/S)-(b).** TFA (4.4 mL, 57 mmol) was added dropwise to a stirred and ice-chilled solution of (S)-**4** or (R/S)-**4** (1 mmol) in freshly distilled ( $P_2O_5$ )  $CH_2Cl_2$  (3.4 mL). The solution was stirred under these reaction conditions for 5 h and the solvent was removed in vacuo to give (S)-**b** and (R/S)-**b** as solids.

**4.5.11. (S)-N-Hydroxy-2-(N-isopropoxybiphenyl-4-ylsulfonamido)-3-methylbutanamide (S)-(b).** The title compound was prepared from (S)-**4** following the general procedure. White solid (77.3% yield); mp 117–119 °C;  $[\alpha]_D^{20} -31.7$  ( $c$  0.01, MeOH);  $^1H$  NMR ( $CDCl_3$ )  $\delta$ : 0.92 (d,  $J = 6.5$  Hz, 6H); 1.29 (d,  $J = 6.2$  Hz, 3H); 1.36 (d,  $J = 6.2$  Hz, 3H); 2.04 (m, 1H); 3.97 (m, 1H); 4.54 (septet,  $J = 6.2$  Hz, 1H); 7.42–7.53 (m, 3H); 7.58–7.63 (m, 2H); 7.72–7.77 (m, 2H); 7.91–7.95 (m, 2H). Anal. Calcd for  $C_{20}H_{26}N_2O_5S$ : C, 59.09; H, 6.45; N, 6.89. Found: C, 59.21; H, 6.46; N, 6.88.

**4.5.12. (R/S)-N-Hydroxy-2-(N-isopropoxybiphenyl-4-ylsulfonamido)-3-methylbutanamide (R/S)-(b).** The title compound was prepared from (R/S)-**4** following the general procedure. The crude product was recrystallized from  $Et_2O$  and  $n$ -hexane to give (R/S)-**b** (64% yield) as a white solid; mp 132–134 °C;  $^1H$  NMR ( $CDCl_3$ )  $\delta$ : 0.91 (d,  $J = 6.7$  Hz, 6H); 1.30 (d,  $J = 6.2$  Hz, 3H); 1.35 (d,  $J = 6.2$  Hz, 3H); 2.03 (m, 1H); 3.93 (m, 1H); 4.53 (septet,  $J = 6.4$  Hz, 1H); 7.42–7.52 (m, 3H); 7.58–7.63 (m, 2H); 7.72–7.76 (m, 2H); 7.90–7.95 (m, 2H). Anal. Calcd for  $C_{20}H_{26}O_5N_2S$ : C, 59.09; H, 6.45; N, 6.89. Found: C, 59.19; H, 6.47; N, 6.88.

**4.5.13. (S)-2-Acetoxy-3-methylbutanoic acid (S)-(6).** Acetyl chloride (3.43 mL, 48.30 mmol) was slowly added to (S)-(+)-2-hydroxy-3-methylbutanoic acid **5** (2.50 g, 21.0 mmol) maintained in an ice bath to keep the temperature below 10 °C. After the addition, the mixture was left overnight at room temperature and was then evaporated in vacuo at 20 °C, and subsequently at 50 °C with the addition of toluene. Compound **6** (84% yield) was used without further purification. Pale yellow oil;  $[\alpha]_D^{20} -22.2$  ( $c$  0.01, MeOH);  $^1H$  NMR ( $CDCl_3$ )  $\delta$ : 0.99 (d,  $J = 3.4$  Hz, 3H), 1.02 (d,  $J = 3.4$  Hz, 3H), 2.14 (s, 3H), 2.20–2.32 (m, 1H), 4.86 (d,  $J = 4.4$  Hz, 1H), 10.78 (br s, 1H). Anal. Calcd for  $C_7H_{12}O_4$ : C, 52.49; H, 7.55. Found: C, 52.58; H, 7.56.

**4.5.14. (S)-tert-Butyl-2-Hydroxy-3-methylbutanoate (S)-(7).** A solution of **6** (0.66 g, 4.16 mmol) in toluene (8 mL) containing  $N,N$ -dimethylformamide di-*tert*-butyl acetal (4 mL, 16.64 mmol) was heated to 95 °C for 3 h. The solvent was then evaporated and the crude product was purified by flash chromatography on silica gel ( $n$ -hexane/ $EtOAc$ , 4:1) to give the *tert*-butyl ester as an oil. A solution of LiOH (0.03 g, 1.31 mmol) in  $H_2O$  (2.6 mL) was added to a solution of the *tert*-butyl ester (0.28 g, 1.31 mmol) in MeOH (2.6 mL) and THF (1.3 mL) at 0 °C. After the addition, the mixture was stirred for 3 h at room temperature, then diluted with

$H_2O$ , saturated with NaCl and extracted with  $Et_2O$ . The combined ethereal extracts were dried over anhydrous  $Na_2SO_4$ , filtered and evaporated under reduced pressure to afford **7** as a yellow oil, which solidified on standing (87.8% yield); mp 28–29 °C;  $[\alpha]_D^{20} +1.6$  ( $c$  0.01, MeOH);  $^1H$  NMR ( $CDCl_3$ )  $\delta$ : 0.83 (d,  $J = 6.7$  Hz, 3H), 0.99 (d,  $J = 6.7$  Hz, 3H), 1.47 (s, 9H), 1.95–2.10 (m, 1H), 2.78 (br s, 1H), 3.89 (d,  $J = 3.3$  Hz, 1H). Anal. Calcd for  $C_9H_{18}O_3$ : C, 62.04; H, 10.41. Found: C, 62.12; H, 10.43.

**4.5.15. (R)-tert-Butyl 2-(N-isopropoxybiphenyl-4-ylsulfonamido)-3-methylbutanoate (R)-(8).** Diethyl azodicarboxylate (DEAD) (0.42 mL, 2.71 mmol) was added dropwise to a solution containing (S)-**7** (2.71 mmol), sulfonamide **1** (2.71 mmol) and triphenylphosphine (0.71 g, 2.71 mmol) in anhydrous THF (48 mL) under nitrogen atmosphere at 0 °C. The resulting mixture was stirred for 5 h at 0 °C and evaporated under reduced pressure to afford a crude product, which was purified by flash chromatography on silica gel ( $n$ -hexane/ $EtOAc$ , 20:1), to give (R)-**8** (53% yield) as a yellow oil.  $R_f = 0.29$ ;  $[\alpha]_D^{20} +90.4$  ( $c$  0.01, MeOH);  $^1H$  NMR ( $CD_3COCD_3-d_6$ )  $\delta$ : 0.89 (d,  $J = 6.4$  Hz, 6H), 1.11 (br s, 9H), 1.24 (d,  $J = 6.6$  Hz, 3H), 1.29 (d,  $J = 6.4$  Hz, 3H), 2.25 (m, 1H), 3.77 (d,  $J = 10.4$  Hz, 1H), 4.44 (septet, 1H), 7.45–7.58 (m, 3H), 7.72–7.77 (m, 2H), 7.90–7.94 (m, 2H), 8.00–8.04 (m, 2H). Anal. Calcd for  $C_{24}H_{33}NO_5S$ : C, 64.40; H, 7.43; N, 3.13. Found: C, 64.51; H, 7.44; N, 3.13.

**4.5.16. (R)-2-(N-Isopropoxybiphenyl-4-ylsulfonamido)-3-methylbutanoic acid (R)-(2).** TFA (4.4 mL, 57.3 mmol) was added dropwise to a stirred solution of *tert*-butyl ester (R)-**8** (1 mmol) in freshly distilled  $CH_2Cl_2$  (3.4 mL), cooled to 0 °C. The solution was stirred for 5 h at 0 °C and the solvent was removed in vacuo to give a solid. The crude product was triturated with  $n$ -hexane to give (R)-**2** (78% yield) as a white crystalline solid. Mp 162–163 °C;  $[\alpha]_D^{20} +101.7$  ( $c$  0.01, MeOH);  $^1H$  NMR ( $CDCl_3$ )  $\delta$ : 0.91 (d,  $J = 6.4$  Hz, 6H), 1.24 (d,  $J = 6.2$  Hz, 3H), 1.30 (d,  $J = 6.2$  Hz, 3H), 2.09–2.17 (m, 1H), 3.90 (d,  $J = 10.2$  Hz, 1H), 4.48 (septet, 1H), 5.11 (br s, 1H), 7.42–7.53 (m, 3H), 7.59–7.64 (m, 2H), 7.67–7.72 (m, 2H), 7.91–7.96 (m, 2H). Anal. Calcd for  $C_{20}H_{25}NO_5S$ : C, 61.36; H, 6.44; N, 3.58. Found: C, 61.40; H, 6.44; N, 3.57.

**4.5.17. Preparation of diastereoisomeric amide (R,S)-3 from enantiomerically enriched acid (R)-2.** (R,S)-**3** was re-synthesized as reported above from the enantiomerically enriched acid (R)-**2**.

HPLC: (R,S) amide:  $t_R = 51.2$  min (95.5%); (S,S) amide:  $t_R = 52.8$  min; (4.5%), de 91%.  $F = 0.5 \mu L/min$ ; eluent MeOH/ $H_2O$ , 73:27.

**4.5.18. (R)-N-(tert-Butyldimethylsilyloxy)-2-(N-isopropoxybiphenyl-4-ylsulfonamido)-3-methylbutanamide (R)-(4).** 1-[3-(Dimethylamino)propyl]-3-ethyl carbodiimide hydrochloride (EDCI) was added portionwise to a solution of the carboxylic acid (R)-**2** (1 mmol) and *O*-(*tert*-butyldimethylsilyl)hydroxylamine (147.3 mg, 1 mmol) in freshly distilled  $CH_2Cl_2$  (18 mL) cooled to 0 °C,

(191.7 mg, 1 mmol). After stirring at room temperature for 20 h, the mixture was washed with H<sub>2</sub>O and the organic phase was dried and evaporated in vacuo. The residue was purified by flash chromatography on silica gel (*n*-hexane/EtOAc, 5:1) to give (*R*)-**4** (30% yield) as a white solid. <sup>1</sup>H NMR (CDCl<sub>3</sub>) δ: 0.064 (s, 6H), 0.84 (s, 9H), 0.91–1.01 (m, 6H), 1.23–1.27 (m, 6H), 2.17 (m, 1H), 3.77 (d, *J* = 10.8 Hz, 1H), 4.39 (septet, 1H), 7.41–7.54 (m, 3H), 7.58–7.64 (m, 2H), 7.74–7.78 (m, 2H), 7.94–7.98 (m, 2H), 8.18 (br s, 1H). Anal. Calcd for C<sub>26</sub>H<sub>40</sub>N<sub>2</sub>O<sub>5</sub>SSi: C, 59.97; H, 7.74; N, 5.38. Found: C, 59.99; H, 7.75; N, 5.37.

**4.5.19. (*R*)-*N*-Hydroxy-2-(*N*-isopropoxybiphenyl-4-ylsulfonamido)-3-methylbutanamide (*R*)-**(b)**.** TFA (4.4 mL, 57.3 mmol) was added dropwise to a stirred solution of *O*-(*tert*-butyldimethylsilyl)hydroxamate (*R*)-**4** (1 mmol) in freshly distilled dichloromethane (3.4 mL), cooled to 0 °C. The solution was stirred for 5 h at 0 °C and the solvent was removed in vacuo to give a solid. The crude product was recrystallized from Et<sub>2</sub>O and *n*-hexane to give (*R*)-**b** (48% yield) as a white solid; mp 114–115 °C;  $[\alpha]_D^{20} +94$  (*c* 0.01, CHCl<sub>3</sub>); ee = 91% (*R*); <sup>1</sup>H NMR (CDCl<sub>3</sub>) δ: 0.93 (d, *J* = 6.6 Hz, 6H), 1.30 (d, *J* = 6.2 Hz, 3H), 1.36 (d, *J* = 6.4 Hz, 3H), 2.04 (m, 1H), 3.94 (m, 1H), 4.54 (septet, 1H), 7.42–7.53 (m, 3H), 7.59–7.63 (m, 2H), 7.73–7.77 (m, 2H), 7.91–7.95 (m, 2H); EI-MS, *m/z*: 152 (45); 202 (71); 364 (18); 407 (100); 408 (*M*+1, 23). Anal. Calcd for C<sub>20</sub>H<sub>26</sub>N<sub>2</sub>O<sub>5</sub>S: C, 59.09; H, 6.45; N, 6.89. Found: C, 59.19; H, 6.54; N, 6.86.

**4.5.20. MMP inhibition assays.** Type I procollagenase (pro-MMP-1, human recombinant) was purchased from Calbiochem; recombinant human Progelatinase A (pro-MMP-2, from transfected mouse myeloma cells) was prepared in our laboratory.<sup>1</sup> Proenzymes were activated immediately prior to use with *p*-aminophenylmercuric acetate (APMA 2 mM for 1 h at 37 °C for MMP-2 and 1 mM for 2 h at 37 °C for MMP-1). For assay measurements, the inhibitor stock solutions (DMSO, 100 mM) were further diluted, at seven different concentrations (0.01 nM–300 μM) for each MMP in the fluorimetric assay buffer (FAB: Tris 50 mM, pH 7.5, NaCl 150 mM, CaCl<sub>2</sub> 10 mM, Brij 35 0.05% and DMSO 1%). The activated enzymes (final concentration 0.5 nM for MMP-1 and 2.8 nM for MMP-2) and the inhibitor solutions were incubated in the assay buffer for 4 h at 25 °C. After the addition of 200 μM solution of the fluorogenic substrates (Mca-Lys-Pro-Leu-Gly-Leu-Dap (Dnp)-Ala-Arg-NH<sub>2</sub> for MMP-1 and Mca-Pro-Leu-Gly-Leu-Dpa-Ala-Arg-NH<sub>2</sub> for MMP-2) in DMSO (final concentration 2 μM), the hydrolysis was monitored every 15 s for 10 min, recording the increase in fluorescence ( $\lambda_{\text{ex}}$  = 328 nm,  $\lambda_{\text{em}}$  = 393 nm) using a Molecular Device M-2 Gemini plate reader. The assays were performed in quadruplicate in a total volume of 200 μL per well in 96-well microtitre plates (Corning, black, NBS). Control wells lacked the inhibitor. The MMP inhibition activity was expressed in relative fluorescent units (RFU). The percentage of inhibition was calculated from control reactions without the inhibitor. The IC<sub>50</sub> was determined by using the formula:  $V_i/V_o = 1/(1 + [I]/IC_{50})$ , where  $V_i$  is the initial velocity of

substrate cleavage in the presence of the inhibitor at concentration  $[I]$  and  $V_o$  is the initial velocity in the absence of the inhibitor. Results were analyzed using SoftMax Pro software and GraFit software.<sup>86,87</sup>

## References and notes

- Rossello, A.; Nuti, E.; Carelli, P.; Orlandini, E.; Macchia, M.; Nencetti, S.; Zandomenighi, M.; Balzano, F.; Uccello-Barretta, G.; Albini, A.; Benelli, R.; Cercignani, G.; Murphy, G.; Balsamo, A. *Bioorg. Med. Chem. Lett.* **2005**, *15*, 1321.
- <http://www.clip.ubc.ca>.
- Smith, H. J.; Simons, C. In *Proteinase Peptidase Inhibition: Recent Potential Targets for Drug Development*; Taylor and Francis: London and New York, 2002.
- Folgueras, A. R.; Pendas, A. M.; Sanchez, L. M.; Lopez-Otin, C. *Int. J. Dev. Biol.* **2004**, *48*, 411–424.
- Sternlicht, M. D.; Werb, Z. *Ann. Rev. Cell Dev. Biol.* **2001**, *17*, 463–516.
- Woessner, J. F., Jr.; Nagase, H. *Matrix Metalloproteinases and Timps*; Oxford University Press: Oxford, 2000, pp 1–223.
- Supuran, C. T.; Scozzafava, A. In *Proteinase and Peptidase Inhibition: Recent Potential Targets for Drug Development*; Smith, H. J., Simons, C., Eds.; Taylor and Francis: London and New York, 2002; pp 35–61.
- Whittaker, M.; Floyd, C. D.; Brown, P.; Gearing, A. J. H. *Chem. Rev.* **1999**, *99*, 2735–2776.
- Supuran, C. T.; Casini, A.; Scozzafava, A. *Med. Res. Rev.* **2003**, *23*, 535–558.
- Coussens, L. M.; Fingleton, B.; Matrisian, L. *Science* **2002**, *295*, 2387–2392.
- Purcell, W. T.; Ettinger, D. S. *Curr. Oncol. Rep.* **2003**, *5*, 114–125.
- Wielockx, B.; Libert, C.; Wilson, C. *Cytokine Growth Factor Rev.* **2004**, *15*, 111–115.
- Wada, C. K. *Curr. Top. Med. Chem.* **2004**, *4*, 1255–1267.
- Hanessian, S. *Curr. Top. Med. Chem.* **2004**, *4*, 1269–1287.
- Puerta, D. T.; Cohen, S. M. *Curr. Top. Med. Chem.* **2004**, *4*, 1551–1573.
- Rush, T. S., third; Powers, R. *Curr. Top. Med. Chem.* **2004**, *4*, 1311–1327.
- Skiles, J. W.; Gonnella, N. C.; Jeng, A. Y. *Curr. Med. Chem.* **2004**, *11*, 2911–2977.
- Puerta, D. T.; Lewis, J. A.; Cohen, S. M. *J. Am. Chem. Soc.* **2004**, *126*, 8388–8389.
- Rao, B. G. *Curr. Pharm. Des.* **2005**, *11*, 295–322.
- Maskos, K. *Biochimie* **2005**, *87*, 249–263.
- Cuniasse, P.; Devel, L.; Makaritis, A.; Beau, F.; Georgiadis, D.; Matziari, M.; Yiotakis, A.; Dive, V. *Biochimie* **2005**, *87*, 393–402.
- Itoh, Y.; Nagase, H. *Essays Biochem.* **2002**, *38*, 21–36.
- Sounni, N. E.; Janssen, M.; Foidart, J. M.; Noel, A. *Matrix Biol.* **2003**, *22*, 55–61.
- Sato, H.; Takino, T.; Miyamori, H. *Cancer Sci.* **2005**, *96*, 212–217.
- Cowan, K. N.; Jones, P. L.; Rabinovitch, M. *Circ. Res.* **1999**, *84*, 1223–1233.
- Jones, P. L.; Crack, J.; Rabinovitch, M. *J. Cell. Block.* **1997**, 279–293.
- Eguchi, P. J.; Dempsey, G. D.; Frank, G. D.; Motley, D.; Inagami, T. *J. Biol. Chem.* **2001**, *276*, 7957–7962.
- Ahonen, M.; Poukkula, M.; Baker, A. H.; Kashiwagi, M.; Nagase, H.; Eriksson, J. E.; Kähäri, V. M. *Oncogene* **2003**, *22*, 2121–2134.
- Borkakoti, N. *Biochem. Soc. Trans.* **2004**, *32*, 17–19.

30. Hutchinson, J. W.; Tierney, G. M.; Parson, S. L.; Davis, T. R. C. *J. Bone Joint Surg.* **1998**, *80*, 907–908.
31. Holmbeck, K.; Bianco, P.; Caterina, J.; Yamada, S.; Kromer, M.; Kuznetsov, S. A.; Mankani, M.; Robey, P. G.; Poole, A. R.; Pidoux, I.; Ward, J. M.; Birkedal-Hansen, H. *Cell* **1999**, *99*, 81–92.
32. Steward, W. P. *Cancer Chemother. Pharmacol.* **1999**, *43*, S56–S60.
33. Dahlberg, L.; Billingham, R. C.; Manner, P.; Nelson, F.; Webb, G.; Ionescu, M.; Reiner, A.; Tanzer, M.; Zukor, D.; Chen, J.; Van Wart, H. E.; Poole, A. R. *Arthritis Rheum.* **2000**, *43*, 673–682.
34. Scatena, R. *Expert Opin. Invest. Drugs* **2000**, *9*, 2159–2165.
35. Wada, C. K.; Holms, J. H.; Curtin, M. L.; Dai, Y.; Florjancic, A. S.; Garland, R. B.; Guo, Y.; Heyman, H. R.; Stacey, J. R.; Steinman, D. H.; Albert, D. H.; Bouska, J. J.; Elmore, I. N.; Goodfellow, C. L.; Marcotte, P. A.; Tapang, P.; Morgan, D. W.; Michaelides, M. R.; Davidsson, S. K. *J. Med. Chem.* **2002**, *45*, 219–232.
36. Zook, S. E.; Dagnino, R. Jr.; Deason, M. E.; Bender, S. L.; Melnick, M. J. WO Patent 97/20824, 1997; 127, 108945; *Chem. Abstr.* **1995**, *123*, 2870.
37. Kruger, A.; Arlt, M. J.; Gerg, M.; Kopitz, C.; Bernardo, M. M.; Chang, M.; Mobashery, S.; Fridman, R. *Cancer Res.* **2005**, *65*, 3523–3526.
38. Turpeenniemi-Hujanen, T. *Biochimie* **2005**, *87*, 287–297.
39. Haubner, R.; Wester, H. J. *Curr. Pharm. Des.* **2004**, *10*, 1439–1455.
40. Morgunova, E.; Tuuttila, A.; Bergmann, U.; Isupov, M.; Lindqvist, Y.; Schneider, G.; Tryggvason, K. *Science* **1999**, *284*, 1667–1670.
41. Spurlino, J. C.; Smallwood, A. M.; Carlton, D. D.; Banks, T. M.; Vavra, K. J.; Johnson, J. S.; Cook, E. R.; Falvo, J.; Wahl, R. C.; Pulvino, T. A.; Wendoloski, J. J.; Smith, D. L. *Proteins* **1994**, *19*, 98–109.
42. Leung, D.; Abbenante, G.; Fairlie, D. P. *J. Med. Chem.* **2000**, *72*, 305–341.
43. Babine, R. E.; Bender, S. L. *Chem. Rev.* **1997**, *97*, 1359–1472.
44. Coussens, L. M.; Fingleton, B.; Matrisian, L. M. *Science* **2002**, *295*, 2387–2390.
45. Oreola, A.; Donini, T.; Kollman, P. A. *J. Med. Chem.* **2000**, *43*, 4180–4188.
46. Browner, M. F.; Smith, W. W. *Biochemistry* **1995**, *34*, 6602–6610.
47. Rowsell, S.; Hawatin, P.; Minshull, C. A.; Jepson, H.; Brockbank, S. M. V.; Barratt, D. G.; Slater, A. M.; McPheat, W. L.; Waterson, D.; Henney, A. M.; Paupit, R. A. *J. Mol. Biol.* **2002**, *319*, 173–181.
48. Rossello, A.; Nuti, E.; Orlandini, E.; Carelli, P.; Rapposelli, S.; Macchia, M.; Minutolo, F.; Carbonaro, L.; Albin, A.; Benelli, R.; Cercignani, G.; Murphy, G.; Balsamo, A. *Bioorg. Med. Chem.* **2004**, *12*, 2441–2450.
49. Cheng, F.; Zhang, R.; Luo, X.; Shen, J.; Li, X.; Gu, J.; Zhu, W.; Shen, J.; Sagi, I.; Ji, R.; Chen, K.; Jiang, H. *J. Phys. Chem. B* **2002**, *106*, 4552–4559.
50. Hu, X.; Shelver, W. H. *J. Mol. Graphics Modell.* **2003**, *22*, 115–126.
51. Hu, X.; Balaz, S.; Shelver, W. H. *J. Mol. Graphics Modell.* **2004**, *22*, 293–307.
52. Hanessian, S.; Moitessier, N.; Therrien, E. *J. Comput. Aided Mol. Des.* **2001**, *15*, 1873–1881.
53. Donini, O. A.; Kollman, P. A. *J. Med. Chem.* **2000**, *43*, 4180–4188.
54. Falconi, M.; Altobelli, G.; Io vino, M. C.; Politi, V.; Desideria, A. *J. Comput. Aided Mol. Des.* **2003**, *17*, 837–848.
55. Terp, G. E.; Christensen, I. T.; Jorgensen, F. S. *J. Biomol. Struct. Dyn.* **2000**, *17*, 933–946.
56. Toba, S.; Damodaran, K. V.; Merz, K. M., Jr. *J. Med. Chem.* **1999**, *8*, 1225–1234.
57. Weiner, S. J.; Kollman, P. A.; Case, D. A.; Singh, U. C.; Ghio, C.; Alagona, G.; Profeta, S. J.; Weiner, P. *J. Am. Chem. Soc.* **1984**, *106*, 765–784.
58. Ryde, U. *J. Comput. Aided Mol. Des.* **1996**, *10*, 153–164.
59. Ryde, U. *Biophys. J.* **1999**, *77*, 2777–2787.
60. Torrent, M.; Vreven, T.; Musaev, D. G.; Morokuma, K.; Farkas, Ö.; Schlegel, H. B. *J. Am. Chem. Soc.* **2002**, *124*, 192–193.
61. Olsen, L.; Antony, J.; Hemmingsen, L. *J. Phys. Chem. A* **2002**, *106*, 1046–1053.
62. Rizzo, R. C.; Toba, S.; Kuntz, I. D. *J. Med. Chem.* **2004**, *47*, 3065–3074.
63. Merz, K. M. *J. Am. Chem. Soc.* **1991**, *113*, 406–411.
64. Borkakoti, N.; Winkler, F. K.; Williams, D. H.; D'Arcy, A.; Broadhurst, M. J.; Brown, P. A.; Johnson, W. H.; Murray, E. *J. Nat. Struct. Biol.* **1994**, *1*, 106–110.
65. Lovejoy, B.; Welch, A. R.; Carr, S.; Luong, C.; Broka, C.; Hendricks, R. T.; Campbell, J. A.; Walker, K. A.; Martin, R.; Van Wart, H.; Browner, M. F. *Nat. Struct. Biol.* **1999**, *6*, 217–221.
66. Dhanaraj, V.; Williams, M. G.; Ye, Q. Z.; Molina, F.; Johnson, L. L.; Ortwine, D. F.; Pavlovsky, A.; Rubin, J. R.; Skeean, R. W.; White, A. D.; Humblet, C.; Hupe, D. J.; Blundell, T. L. *Croat. Chem. Acta* **1999**, *72*, 575–591.
67. GRID v. 22 Molecular Discovery Ltd (<http://www.moldiscovery.com>).
68. Eliel, E. L.; Wilen, S. H.; Mander, L. N. In *Stereochemistry of Organic Compounds*; John Wiley and Sons Inc.: New York, 1994; pp 153–275.
69. Dan, Y.; Bing, L.; Fei-Fu, N.; Yi-Long, Y.; Jin, Q.; Yun-Dong, W. *J. Org. Chem.* **2001**, *66*, 7303.
70. Rosini, C.; Uccello-Barretta, G.; Pini, D.; Abete, C.; Salvadori, P. *J. Org. Chem.* **1988**, *53*, 4579–4581.
71. Gaussian 98, a.5. Frisch, M. J.; Trucks, G. W.; Schlegel, H. B.; Scuseria, G. E.; Robb, M. A.; Cheeseman, J. R.; Zakrzewski, V. G.; Montgomery, J. A.; Stratmann, R. E.; Burant, J. C.; Dapprich, S.; Millam, J. M.; Daniels, A. D.; Kudin, K. N.; Strain, M. C.; Farkas, O.; Tomasi, J.; Barone, V.; Cossi, M.; Cammi, R.; Mennucci, B.; Pomelli, C.; Adamo, C.; Clifford, S.; Ochterski, J.; Petersson, G. A.; Ayala, P. Y.; Cui, Q.; Morokuma, K.; Malick, D. K.; Rabuck, A. D.; Raghavachari, K.; Foresman, J. B.; Cioslowski, J.; Ortiz, J. V.; Stefanov, B. B.; Liu, G.; Liashenko, A.; Piskorz, P.; Komaromi, I.; Gomperts, R.; Martin, R. L.; Fox, D. J.; Keith, T.; Al-Laham, M. A.; Peng, C. Y.; Nanayakkara, A.; Gonzalez, C.; Challacombe, M.; Gill, P. M. W.; Johnson, B. G.; Chen, W.; Wong, M. W.; Andres, J. L.; Head-Gordon, M.; Replogle, E. S.; Pople, J. A. Gaussian, Inc., Pittsburgh PA, 1998.
72. Bauschlicher, C. W. *Chem. Phys. Lett.* **1995**, *246*, 40–44.
73. Ricca, A.; Bauschlicher, C. W. *Theor. Chim. Acta* **1995**, *92*, 123–131.
74. Becke, D. *Phys. Rev. A* **1988**, *38*, 3098–3100.
75. Lee, C.; Yang, W.; Parr, R. G. *Phys. Rev. B* **1988**, *37*, 785–789.
76. Miehlich, B.; Savin, A.; Stoll, H.; Preuss, H. *Chem. Phys. Lett.* **1989**, *157*, 200–206.
77. Hay, P. J.; Wadt, W. R. *J. Chem. Phys.* **1988**, *82*, 299–310.
78. Dunning, T. H., Jr.; Hay, P. J., Eds. In *Modern Theoretical Chemistry*; Schaefer, H. F., III, Ed.; Plenum: New York, 1976; Vol. 3, pp 1–28.
79. Antony, J.; Hansen, B.; Hemmingsen, L.; Bauer, R. *J. Phys. Chem. A* **2000**, *104*, 6047–6055.
80. Bayly, C. I.; Cieplak, P.; Cornell, W. D.; Kollman, P. A. *J. Phys. Chem.* **1993**, *97*, 10269–10280.
81. Amber version 8.0; University of California at San Francisco: San Francisco, CA.



82. Darden, T.; Darrin, Y.; Pedersen, L. *J. Chem. Phys.* **1993**, 98, 10089–10092.
83. Berman, H. M.; Westbrook, J.; Feng, Z.; Gilliland, G.; Bhat, T. N.; Weissig, H.; Shindyalov, I. N.; Bourne, P. E. *Nucleic Acids Res.* **2000**, 28, 235–242.
84. Grams, F.; Crimmin, M.; Hinnes, L.; Huxley, P.; Pieper, M.; Tschesche, H.; Bode, W. *Biochemistry* **1995**, 34, 14012–14020.
85. Munie, G.; McDonald, J. J.; Stevens, A. M.; Howard, C. P.; De Crescenzo, G. A.; Welsch, D.; Shieh, H. S.; Stallings, W. C. *Biochim. Biophys. Acta* **2002**, 1598, 10–23.
86. SoftMax Pro 4.7.1 by Molecular Device.
87. GraFit version 4 by Erithecus Software.
88. Beckett, R. P.; Whittaker, M. *Exp. Opin. Ther. Patents* **1998**, 8, 259–282.